BNL-213693-2020-JAAM

Structure and Chemical State of Cesium on Well-Defined Cu(111) and Cu2O/Cu(111) Surfaces

R. C. Hamlyn, S. D. Senanayake

To be published in "JOURNAL OF PHYSICAL CHEMISTRY C"

February 2020

Chemistry Department

Brookhaven National Laboratory

U.S. Department of Energy

USDOE Office of Science (SC), Basic Energy Sciences (BES) (SC-22)

Notice: This manuscript has been authored by employees of Brookhaven Science Associates, LLC under Contract No. DE-SC0012704 with the U.S. Department of Energy. The publisher by accepting the manuscript for publication acknowledges that the United States Government retains a non-exclusive, paid-up, irrevocable, world-wide license to publish or reproduce the published form of this manuscript, or allow others to do so, for United States Government purposes.

DISCLAIMER

This report was prepared as an account of work sponsored by an agency of the United States Government. Neither the United States Government nor any agency thereof, nor any of their employees, nor any of their contractors, subcontractors, or their employees, makes any warranty, express or implied, or assumes any legal liability or responsibility for the accuracy, completeness, or any third party's use or the results of such use of any information, apparatus, product, or process disclosed, or represents that its use would not infringe privately owned rights. Reference herein to any specific commercial product, process, or service by trade name, trademark, manufacturer, or otherwise, does not necessarily constitute or imply its endorsement, recommendation, or favoring by the United States Government or any agency thereof or its contractors or subcontractors. The views and opinions of authors expressed herein do not necessarily state or reflect those of the United States Government or any agency thereof.

Structure and Chemical State of Cesium on Well-Defined Cu(111) and Cu_2O/Cu(111) Surfaces

Rebecca C. E. Hamlyn,[1] Mausumi Mahapatra,[2] Ivan Orozco,[1] Iradwikanari Waluyo,[3] Adrian Hunt,[3] José Rodriguez,[1,2] Michael G.White,[1,2,*] and Sanjaya D. Senanayake, [2*]

[1] Chemistry Department, Stony Brook University, Stony Brook, NY 11794 USA

[2] Chemistry Department, Brookhaven National Laboratory, Upton, NY 11973 USA

[3] National Synchrotron Light Source II, Brookhaven National Laboratory, Upton, NY 11973 USA

Corresponding Authors: * SDS, ssnanay@bnl.gov; MGW, mgwhite@bnl.gov; Bldg. 555A, Brookhaven National Laboratory, P.O. Box 5000, Upton, NY 11973-5000

ABSTRACT

The deposition of cesium (Cs) onto the metallic and oxidized surfaces of Cu(111) was investigated using scanning tunneling microscopy (STM), X-ray photoelectron spectroscopy (XPS) and density functional theory calculations (DFT) to elucidate the properties of alkali metals when supported on metal and oxide surfaces. At low coverages, cesium adopts partially cationic ($Cs^{\delta+}$), highly mobile and likely atomic structures on the metal surface of Cu(111). Such structures are not observable at room temperature using STM due to rapid surface mobility but can be quantified using XPS. This is further verified by DFT calculations which show that Cs adsorption on Cu(111) is site insensitive, where atop, bridge and hollow sites yield identical adsorption energy. Reaction with O_2 ($1x10^{-7}$ Torr) at room temperature of the Cs/Cu(111) surface results in both CsO_x and Cu_xO formation, initially from the Cs sites and Cu step edges, and then subsequently encompassing the terraces. The presence of Cs promotes the oxidation process by O_2 and we have identified the oxidized $Cs^{\delta+}$ and Cu^{+1} using XPS. In contrast to the metallic substrate, the deposition of Cs onto the pre-oxidized surface of Cu_2O/Cu(111) allows for anchoring of oxidized $Cs^{\delta+}$ nanostructures (few nm) which appear indiscriminately on the oxide surface with high dispersion and low mobility. While clearly distinguishable using STM, we have revealed a rich geometric heterogeneity of the nanostructures of Cs on Cu_2O/Cu(111), likely templated through a strong interaction between the Cs and the Cu_2O substrate. In addition, it is also evident that Cs imparts a destabilizing effect on the ordered oxide substrate, as observed through the increase of surface defects. Finally, the thermal stability of the Cs structures was studied, using sequential annealing steps revealing that Cs remained stable up to 550 K and with some loss of both cesium and oxygenate higher temperatures of 650 K. DFT calculations show that unlike Cu(111), the adsorption energy of Cs on Cu_xO /Cu(111) is highly dependent on adsorption site, and electronic effects affect the interaction between Cs, O and Cu.

KEYWORDS: Cesium, Cu(111), Cu_2O, STM, XPS

INTRODUCTION

Alkali metals represent the simplest of modifiers utilized in a broad range of energy materials, often employed to impart distinct chemistry from the host materials, to achieve distinct functionality. For instance, alkali metals are used as surface additives for the promotion of a wide array of catalytic processes. These processes include reactions such as the water-gas-shift and methanol synthesis over Cu-based catalysts, where alkali metals may be used to lower activation steps or steer carbon selectivity.[1–3] Further, cesium is known to enhance reactions as varied as ammonia synthesis,[4] epoxidation reactions,[5] Fischer-Tropsch synthesis[6,7] and plays a role in C-C coupling functionality.[8–10]

With this motivation, fundamental investigations of alkali metal adsorption on well-defined metallic surfaces have been conducted over the last several decades.[11] This includes Na, K, Cs and Li on substrates such as Ru, W, Fe, Au, Ag, Cu, Ni, Pt, Pd and more.[11–18] Their simple electronic structure makes them a good candidate for systematic adsorption, phase transition and size-dependence studies and for understanding how they act as surface promoters to impart new chemistry from the metal support surface. Alkali metals are known to be very electropositive; hybridization with a transition metal substrate causes a broadening of the valence s-orbital that yields a local work function decrease and partial iconicity.[19] At very small coverages, the alkali can give a full electron to the metal surface, but at large coverages, the ionicity of the alkali-transition metal bond decreases.[4] Early work by Langmuir et al. highlighted alkali behavior on tungsten substrates that prove to be common effects across metal substrates. These include high surface diffusion, a decrease in work function, and a further decrease before increase in work function on these surfaces with addition of oxygen.[20]

Studies of Na, K and Cs on metals such as Ni show that the lower the alkali ionization potential, the larger the work function change and resulting dipole moment of the adsorbed metal alkali.[21] Thus, larger alkalis with a low ionization potential such as cesium will have a larger effective dipole and will induce a larger perturbation of the surrounding electronic environment. This plays out in the surface morphology and alkali adsorption behavior. Low temperature is often needed for successful probe imaging due to low diffusion barriers.[19] At lower coverages, dipole repulsions tend to create a mutual alkali adsorbate distance on metallic substrates. Higher coverage is another means toward improved imaging and is often necessary so as to have enough mutual dipole

repulsion to stabilize long range order.[14] At this threshold, Cs often takes on hexagonally ordered domains on low energy fcc facets such as Ag(111).[14]

Oxide surfaces offer sites that can anchor and activate foreign adatoms in unique ways. Madey et al. summarized early work on the adsorption and desorption of alkalis on oxide surfaces, whose behavior is largely dictated by the band gap size.[22] Wide band gap materials limit the charge transfer of adsorbed alkalis, and seem to be controlled largely by surface defects.[23] On the other side of the spectrum, alkalis on narrow band gap surfaces have a much stronger interaction.[22] At low alkali coverages, charge transfer to the substrate may be fully complete. This is particularly the case for reducible oxides such as TiO_2, in which the surface substrate cation may be reduced from Ti^{4+} to Ti^{3+}.[24] As the coverage increases, the charge transfer is incomplete, as is the case on metallic surfaces. The alkalis Na and K have formed ordered structures on oxides at low coverage, and while LEED structures have not been observed for Cs on TiO_2(110), it is expected that Cs would follow this trend.[24] MIES spectra following the deposition of Cs on TiO_2(110) will gradually change.[25] This has been interpreted as a rearrangement of surface oxygen as the Cs and Ti ions compete for oxygen bonding.[25] What remains unexplored is alkali behavior on thin film oxides and the role of O during the interaction between alkali and the metal surface.

Many cesium-promoted reactions occur over Cu-based catalysts. These include the water gas shift (WGS) reaction,[1,2] alcohol synthesis[3,26] and other C2+ oxygenate reactions.[27] There have been several surface chemistry studies conducted of cesium on various copper facets.[12,28–34] The results follow coverage-dependent charge transfer and work function trends of those discussed above on transition metals. The results also yield coverage-dependent ordered structures of Cs on the metallic surface.[12,35–37] Although cesium can be regarded as a simple modifier via electron donation, its role in heterogeneous catalysis is multifunctional and complex, with effects as a textural, electronic or chemical influencer. An important consideration in the study of alkali promotion is the chemical state of the alkali species. It is understood that oxygen often co-exists with surface alkalis and that transient oxygen species play a role in many reactions.[33,38–40] Oxygen may also accentuate the effect of the alkali metal.[18] For instance, in their study of Cs promotion of the WGS, Campbell and Koel attributed promotional effects to the direct participation of a CsO_x complex.[1] Partially oxidized Cu is also understood to have a critical role in the activity of chemical

conversion.[41] Yet much remains to be understood about the working mechanism of Cs as a promoter for many small molecule conversions.

As many relevant cesium-promoted chemical conversions occur on Cu-based surfaces, and Cu(111) offers a well-studied reversibly oxidizable facet,[42–44] we used this substrate in an effort to better understand how small additions of alkali metals interact with Cu surfaces. We have carried out model studies of cesium over a metallic and oxidized copper surface, examining the behavior and thermal stability. Scanning tunneling microscopy (STM) is used to elucidate the morphology of Cs on both Cu(111) and Cu_2O/Cu(111) surfaces, with chemical identification enabled through high resolution X-ray photoelectron spectroscopy (XPS).

EXPERIMENTAL

STM experiments were carried out in an ultrahigh vacuum (UHV) chamber with a base pressure of ~5 x 10^{-10} Torr containing an Omicron variable temperature microscope. Images were obtained using an etched Pt-Ir (80:20) alloy tip, and analyzed using WSxM software.[45] The XPS experiment for deposition of Cs on metallic copper (Figure 1) was conducted in a SPECS AP-XPS chamber with a base pressure of 1 x 10^{-9} Torr. This chamber is equipped with a PHOIBOS 150 EP MCD-9 analyzer and a Mg Kα anode x-ray source (resolution ~0.5 eV). All spectra were collected with a pass energy of 30 eV and referenced to the Fermi edge. All other XPS experiments were conducted at the 23-ID-2 beamline (IOS) at the National Synchrotron Light Source II at Brookhaven National Laboratory. The analysis chamber is equipped with a SPECS Phoibos 150 NAP analyzer. A full description of the beamline, beam characteristics and end station configuration are reported elsewhere.[46] The XPS data for relevant regions were collected at the following photon energies: 1180 eV for Cu 2p, 910 eV for Cs 3d and 710 eV for O 1s. The resolution is approximately 0.2 to 0.3 eV. Binding energy shifts are referenced to the Fermi edge.

The Cu(111) crystal was prepared by cycles of Ar sputtering and annealing in UHV to ~1000 K until the surface comprised of large, atomically flat terraces, verified with STM. The Cu_2O thin film was grown on the Cu(111) substrate by annealing to 550 K for 10 minutes and cooling back toward room temperature for 10 minutes, both in a background pressure of 5 x 10^{-7} Torr O_2. Cesium was deposited from a Società Apparecchi Elettrici e Scientifici (SAES) commercial getter

source. In STM images, Cs coverage was estimated by the total area percentage (monolayer equivalents, MLE) occupied by the observed protrusions. The STM getter is quite reliable in its deposition rate, and so approximate coverages are also compared via deposition time in all images where the Cs cannot be seen, as is the case on the metallic Cu surface. Coverage in XPS was obtained from both the attenuation of the normalized Cu 2p 3/2 peak intensity and the growth of the Cs 3d peak as proposed by Seah, et al. and Jablonski.[47,48] Coverage was drawn from the linear relationship between the two parameters.

DFT calculations were performed with the projector augmented wave method,[49,50] as implemented in the Vienna Ab-initio simulation package (VASP).[51–53] The Perdew–Wang functional (GGAPW91) within the generalized gradient approximation (GGA) was used to describe exchange–correlation effects.[54] A cut off of 400 eV was used for the planewave basis set, and the wave functions and electron density were converged to within 1×10^{-5} eV. The first Brillouin zone was sampled by 3×3×1 k-points using the Monkhorst-Pack scheme.[55] The conjugate gradient algorithm was used in the geometry optimization method. Geometric relaxations were considered to have converged when the force was < 0.02 eV $Å^{-1}$ on all unrestricted atoms. To model the 29/44 structure, we built a Cu_xO-like O-Cu-O overlayer on top of a three-layer (4x4) Cu(111) slab as described in a previous publication.[56] A Hubbard U correction of U_{eff} = 6.2 eV was applied to the Cu d orbitals of the Cu_xO layer. The adsorbate (cesium) and the top two layer atoms of the Cu(111) and Cu_xO/(Cu(111) slab were allowed to relax while the bottom two layer atoms were fixed during geometry optimization. A vacuum layer of 21 Å is added perpendicular to the Cu(111) and Cu_xO/Cu(111) slab to avoid artificial interaction between the slab and its periodic images. The binding energy (BE) of adsorbate (ads) on the surface is defined as: $BE_{(ads)} = E_{(ads + surface)} - E_{(surface)} - E_{(ads)}$, where $E_{(ads + surface)}$, $E_{(surface)}$ and $E_{(ads)}$ are the total energies of optimized adsorbate + surface, clean surface, and adsorbate in the gas phase, respectively.

RESULTS AND DISCUSSION

1. Cesium deposition on Cu(111)

1.1 Cs onto clean Cu(111)

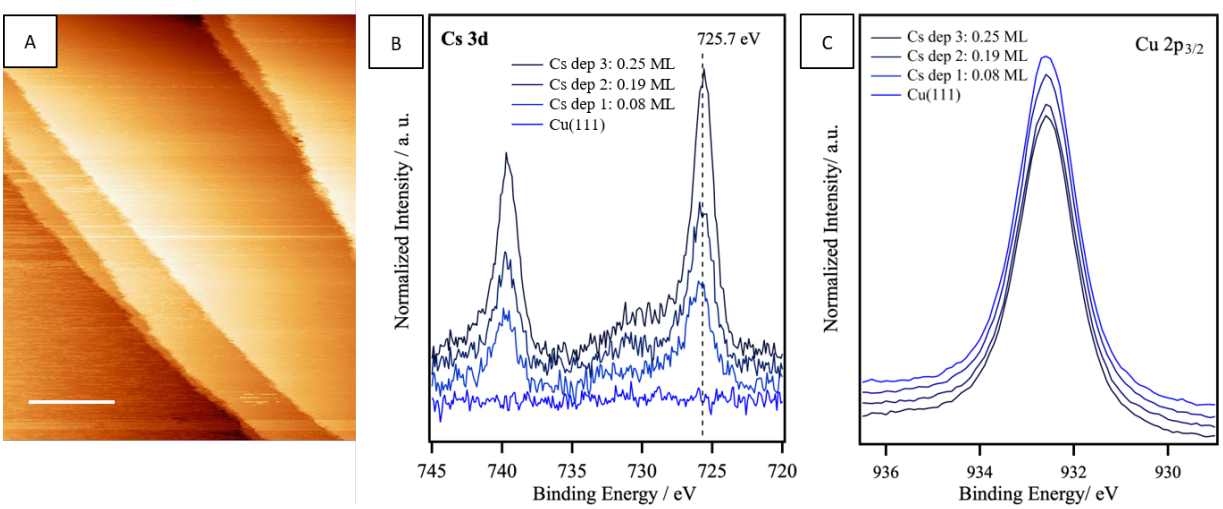

Figure 1: A) STM image of Cs on the Cu(111) surface (10 s. deposition, est. coverage = 0.03 MLE, V_t: -0.5 V, I_t: 0.04 nA). Scale bar = 20 nm. B) and C) Cs 3d and Cu $2p_{3/2}$ XPS spectra, respectively, of sequential depositions of cesium on the Cu(111) surface. Coverages of the spectra for each deposition are estimated to be: 1: 0.08 ML, 2: 0.19 ML, 3: 0.25 ML, determined as described in the experimental section.

Figure 1A depicts a 10 second cesium deposition on the Cu(111) surface in STM corresponding to 0.03 MLE coverage. Cs is too mobile on Cu(111) to be imaged by STM at room temperature, but its presence is detected in the streaking on the surface and fuzzy step edges of the crystal.

Low temperature (< 300 K) studies have followed the deposition of cesium on the Cu(111) surface largely based on diffraction techniques.[28,31,36] It is reported that the cesium first forms a loose structure of randomly distributed adatoms with an approximate mutual distance above 1 nm at very low coverages (< 0.1 ML, defined as Cs_{atom}:Cu_{atom}), and decreasing toward 5.7 Å with addition of more Cs. A gradual compression in the lattice constant continues with higher coverages, yielding an incommensurate layer with rotation angle dependent on the temperature.[36] Saturation of the first layer is achieved at 0.25 ML at room temperature conditions (0.28 ML for 80 K), in which a p(2x2) layer of Cs atoms are packed with a nearest neighbor distance of 5.10 Å (closer than that of bulk Cs at 5.25 Å).[36] These findings were further supported via low temperature

STM.[37] Despite the low temperature elucidation of the Cs behavior, imaging alkalis on transition metal surfaces at room temperature remains elusive due to their notoriously high mobility. This is an effect seen across many such systems above 100 K.[19]

Figure 1B and 1C presents XPS of the Cs 3d and Cu 2p with incremental coverages of Cs onto clean Cu(111) at room temperature. In the Cs 3d region, the 5/2 and 3/2 features are observed at 725.7 eV and 740 eV, respectively, which increase as a function of deposition time. In addition, plasmon loss features develop in the Cs 3d spectra at ~730 eV at higher coverages. This broad feature between 729 and 733 eV grows with coverage, with a large shoulder to the 3d peaks upon the third deposition (Fig. 1B). Lindgren and Wallden described the development of Cs electron loss features, where above a critical coverage of 0.11 ML on Cu, the intensity of the loss peak increases rapidly relative to the elastically scattered electrons of the primary Cs 3d peaks. It is at this point the change from largely ionic character to metallic is thought to be complete.[28,35] This is close to the work function minimum, which they determined via electron loss spectroscopy to occur around 0.14 ML.[12]

In an attempt to better understand the interactions of Cs with the Cu(111), DFT calculations were carried out for 0.06 ML coverage of Cs on three different adsorption sites (atop, bridge and 3-fold hollow) of Cu(111) and is shown in Figure 2. The coverage is defined by the ratio between Cs to surface Cu atoms. Cs on atop, bridge and hollow sites all have identical adsorption energies of -2.45 eV. The identical adsorption energy is a consequence of larger ionic radii of Cs as reported in literature for alkali metal adsorption on Al(111).[57] As a consequence of the larger atomic radius, Cs experiences a rather small substrate electron density corrugation. It is apparent that the high adsorption energy allows the Cs atoms on the surface (as observed in XPS) but does not affect the mobility due to lack of a preferential adsorption site on Cu(111). With minimal diffusion barrier and indiscriminate surface site preference, Cs mobility is likely extremely high for room temperature STM resolution.

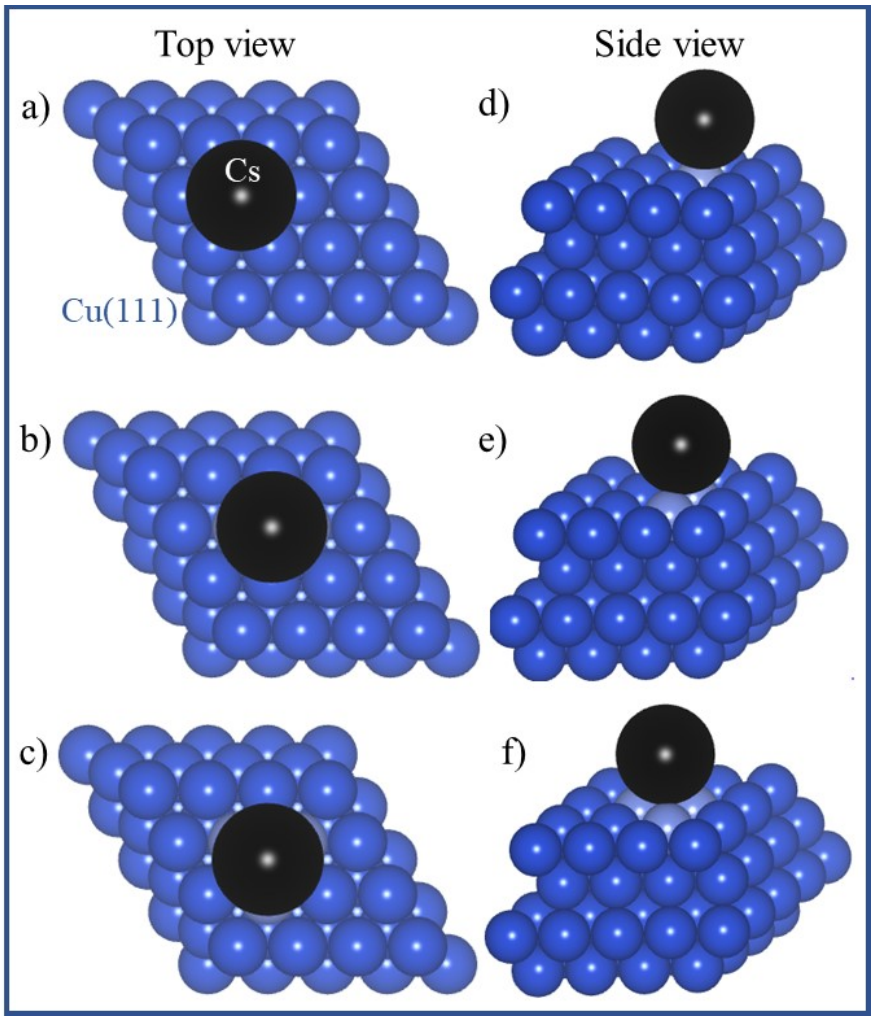

Figure 2: Cs adsorption on Cu(111) on a,d) atop, b,e) bridge and c,f) 3-fold hollow site: The left (a,b,c) and right panel (d,e,f) show the top and side views, respectively. Color representation: dark blue: Cu, black: Cs and the Cu atoms which are directly bonded to Cs are shown in lighter blue.

1.2 Oxidation of Cs/Cu(111)

To assess the kinetics and structure resulting from oxidation of Cs pre-covered Cu(111), we exposed the surface from Figure 1A (10 sec. Cs deposition, ~0.03 MLE) to oxygen at low pressures. The chamber was backfilled with $1x10^{-7}$ Torr O_2 while collecting STM images. These images are shown in Figures 3 and 4, with the exposure indicated in time and in Langmuir (1×10^{-6} Torr·s). Within the first several Langmuir of exposure, the imaging stability improved with less streaking on the surface. On a large scale, oxidation of the cesium pre-covered Cu(111) surface results in formation of surface structures observed in alkali-free Cu(111) oxidation. This includes

oxide nucleation at the step edges, with pseudo-triangular peninsulas and depressions forming in the process.[42,43] A disordered oxide layer grows from the step edge as a mass transfer of copper from the upper terrace is incorporated into this layer. The step edges become jagged and sometimes become triangular islands as the receding step edge leaves them behind.

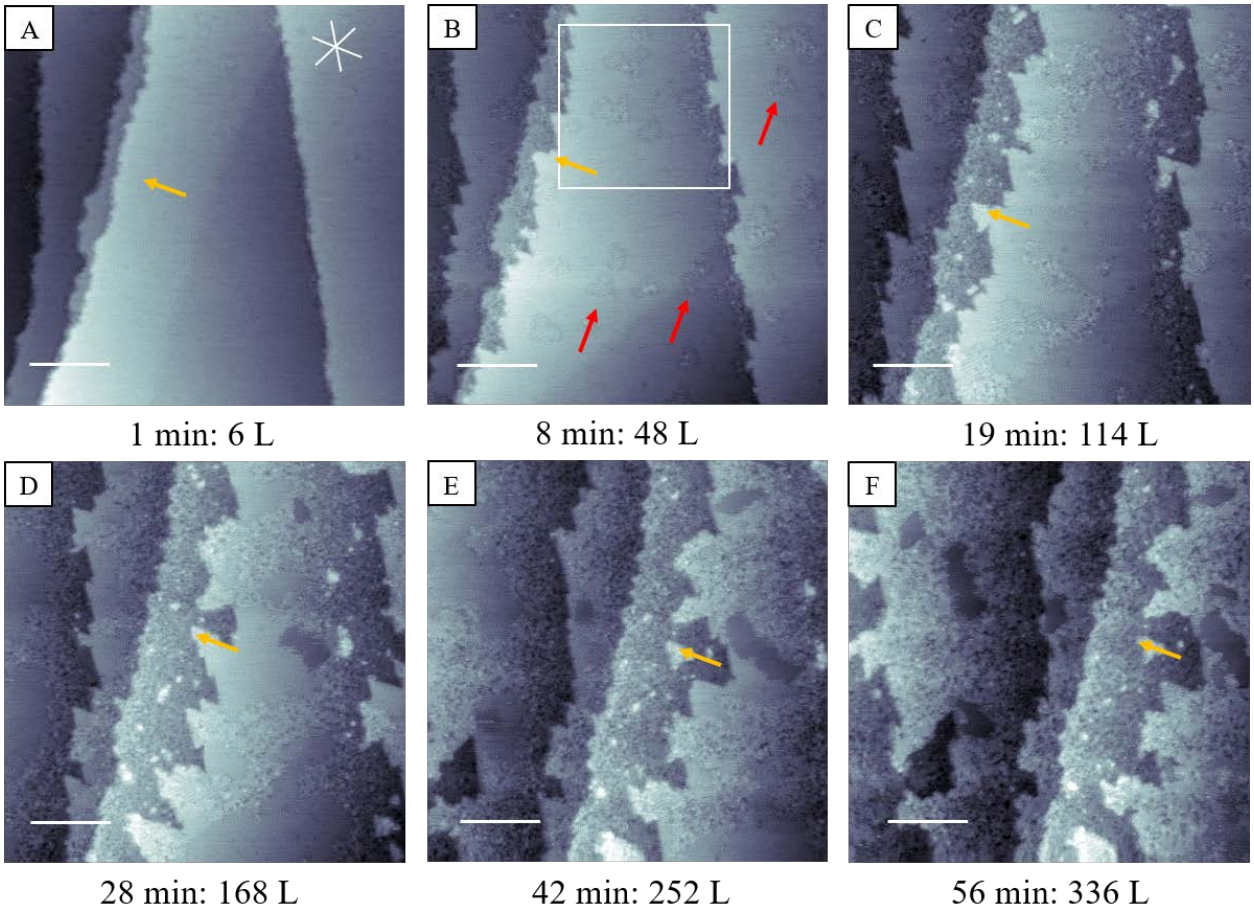

Figure 3: Large scale STM images following the room temperature oxidation of the Cs/Cu(111) surface under 1×10^{-7} Torr O_2. Estimated cesium coverage of 3% by area (10 sec. deposition), V_t: -1.2 V, I_t: 0.1 nA. The time of exposure and O_2 dose in Langmuir is listed below each image. Orange arrows indicate the same position on the surface. Red arrows indicate cesium related oxidation sites, discussed further in Figure 4. The box in the frame B at 48 L indicates the area of focus in Figure 4, in which the contrast is optimized to observe these small terrace features. Scale bars = 20 nm.

Morphological features that suggest the presence of Cs appear on the terraces early in the exposure. Instead of characteristic triangular pits forming on the surface from mass transfer of the Cu atoms,

we first observe a roughening of spots on the terrace indicated by the red arrows in Fig 3B. This suggests that oxidized cesium (CsO_x) is anchoring and serving as a nucleation site for further surface oxidation. Minor triangular pitting, characteristic of room temperature oxidation of Cu(111) as described by Matsumoto et al., is eventually seen in Fig 3D at 168 L exposure.[43]

Figure 4 takes a closer look at these modified terrace sites. Sequential small scale images from the oxidation process follows a region of the Cs pre-covered Cu(111) terraces that is highlighted in the white square of Figure 3B. In the first image at 6 L (Fig 4A), we can see the beginnings of a couple nucleation sites with species in the middle of the terrace, but they remain small and unresolved at this stage. By the next image at 48 L (Fig 4B), these sites have developed into atomically resolved arrays with a high degree of internal order, and the streaking observed in previous scans is largely absent. Further exposures yield a gradual etching into the step edges and a disordered oxide occupies the area where the step edge recedes. As O_2 exposure continues in the later panels (Fig 4D & E), this disordered structure begins to envelope and connect the previously present ordered arrays. There is some diffusion from the outer edges of the arrays as they interact with the growing oxide and fluctuate in shape, however, they remain largely in place and maintain order within this exposure regime.

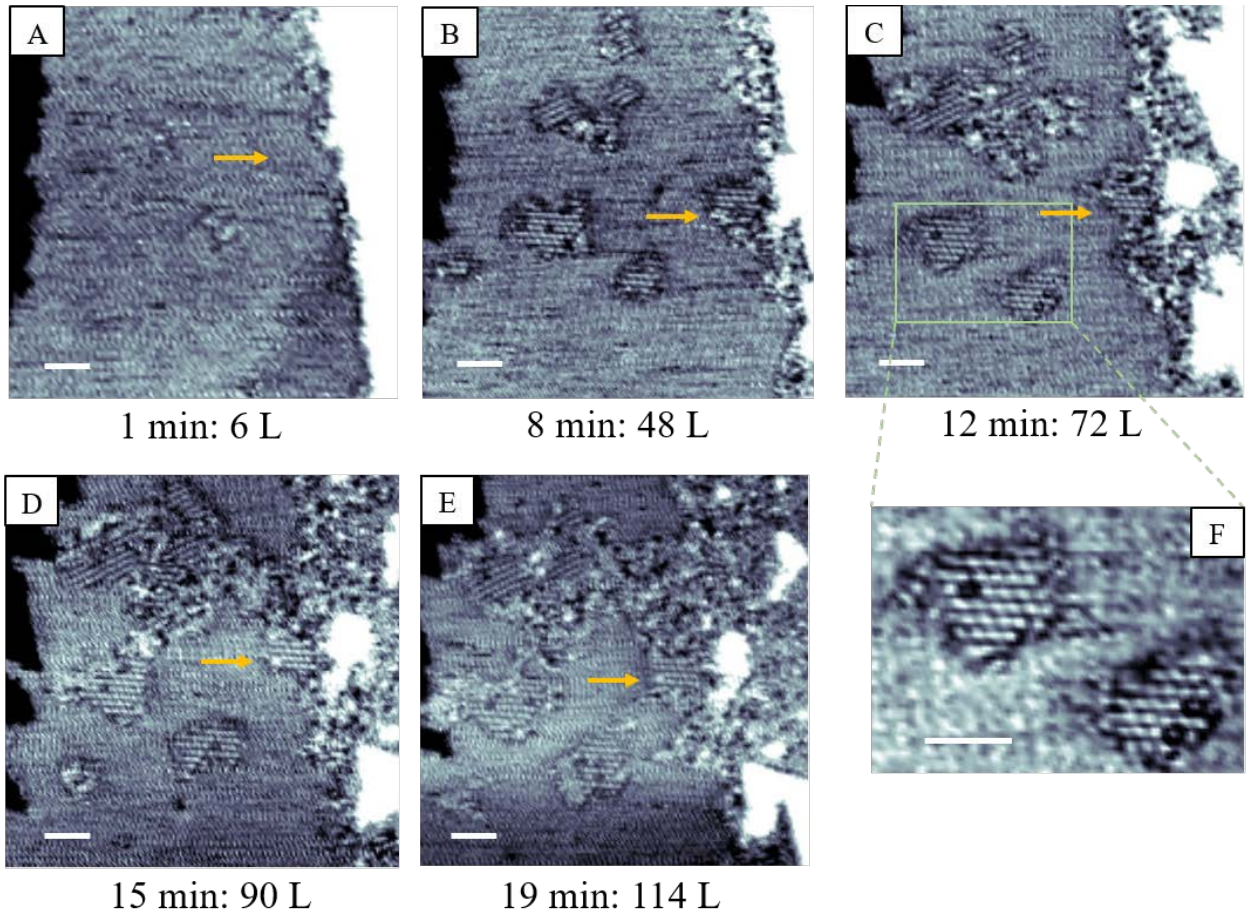

Figure 4: Small scale STM images following the room temperature oxidation of the Cs/Cu(111) surface under 1 x 10^{-7} Torr O_2. Estimated cesium coverage of 0.03 ML by area (10 sec. deposition), V_t: -1.2 V, I_t: 0.1 nA. Orange arrows indicate the same position on the surface. Final image F is an inset from image C at 12 minutes showing more detail of the hexagonally packed structure. Scale bars = 5.0 nm.

Measurements from various orientations of the ordered arrays in Figure 4 yield a close-packed separation of the small unit features of 9.2 +/- 0.3 Å. This is over 1.5 times larger than typical copper oxide spacing, and extend to over 10 nm in some areas, much larger than that of the oxidized copper alone. The structures are found across the substrate and can be rotated 30° from one another, as is seen in the arrays at the top half with respect to the bottom half of Fig 4B-E°. These structures could be a mixed Cs-Cu oxide structure as has been suggested for potassium on oxidized copper.[56] When this was repeated with a higher cesium coverage, the area taken up by the structures scaled with the deposition. This is shown in supplemental figure S1.

The extent of ordering present in these domains is not seen on room temperature Cu(111) surfaces at these lower exposures of oxygen (<100 L O_2). Several early studies found no superstructures formed on the (111) facet below exposures of 10^5 L.[42,58–60] More recently, Matsumoto et al. and Wiame et al. performed thorough probes of Cu(111) oxidation with STM. At exposures higher than what we reach here (e.g. 400 L), Wiame et al. observed only angling of the step edges and triangular pitting of the terraces. They conclude that the oxidation at room temperature and low pressure proceeds only at defect sites corresponding to step edges.[42] Matsumoto et al. were able to achieve higher resolution of the terrace sites and found copper oxide formation within these triangular pits and areas of 'added oxide' on the terraces at exposures of approximately 150 L.[43] There are select areas of loose, hexagonal ordering within these oxide domains. However, they are limited to lateral extensions of 2-3 nm and reported parameters for nearest-neighbor distances are approximately 6.0 Å. They concluded that the tip was probing molecular copper oxide units, and suggested the ordered areas correspond to a structure similar to the top-most layer of $Cu_2O(111)$.[42]

Another indicator of the presence of cesium, is the higher rate of oxidation compared to the cesium-free surface. Following the oxidation process above with XPS in Figure 5, it is clear that Cs facilitates oxidation of the surface. The oxidation of Cu(111) alone yields features of much smaller intensity than the cesiated substrate. O1s peak positions in the right-hand panel of Figure 5 are located around 529.6 eV with a small feature at about 530.6 eV in the orange colored spectra. At lower exposures than necessary for observation in STM, the presence of cesium yields a large increase in the up-take of oxygen over the metallic copper surface, indicating a higher O sticking probability. Exposure of 5 L O_2 oxidizes the cesium, with an energy shift from 726.2 to 725.4 eV and loss of metallic loss features in the Cs 3d panel to the left. A large shift to lower binding energy with addition of oxygen has been reported before in the 5p cesium peaks upon mild oxidation.[61] Lindgren discussed the unusual energy shift effect in cesium oxidation in the late 70s,[61] which has since been ascribed to its Madelung potential.[62] The corresponding 5 L oxygen peak appears at 528.65 eV, lower than that of oxidized copper. This is in agreement with oxidized Cs spectroscopic characteristics on a Cu(110) substrate.[39] As the exposure is increased to 100 L, cesium is further oxidized, shifting the Cs $3d_{5/2}$ peak to 724.8 eV. The oxygen peak continues development at slightly higher binding energy (shift to 529.45 eV), suggesting oxygen is spilling over to the copper surface. Based on the exposure-dependent developments to the O 1s features, we can conclude that

the primary peak has multiple O-species contributions, including those on Cu alone, those at the interface of Cu and Cs, and potentially several oxides formed on Cs clusters.

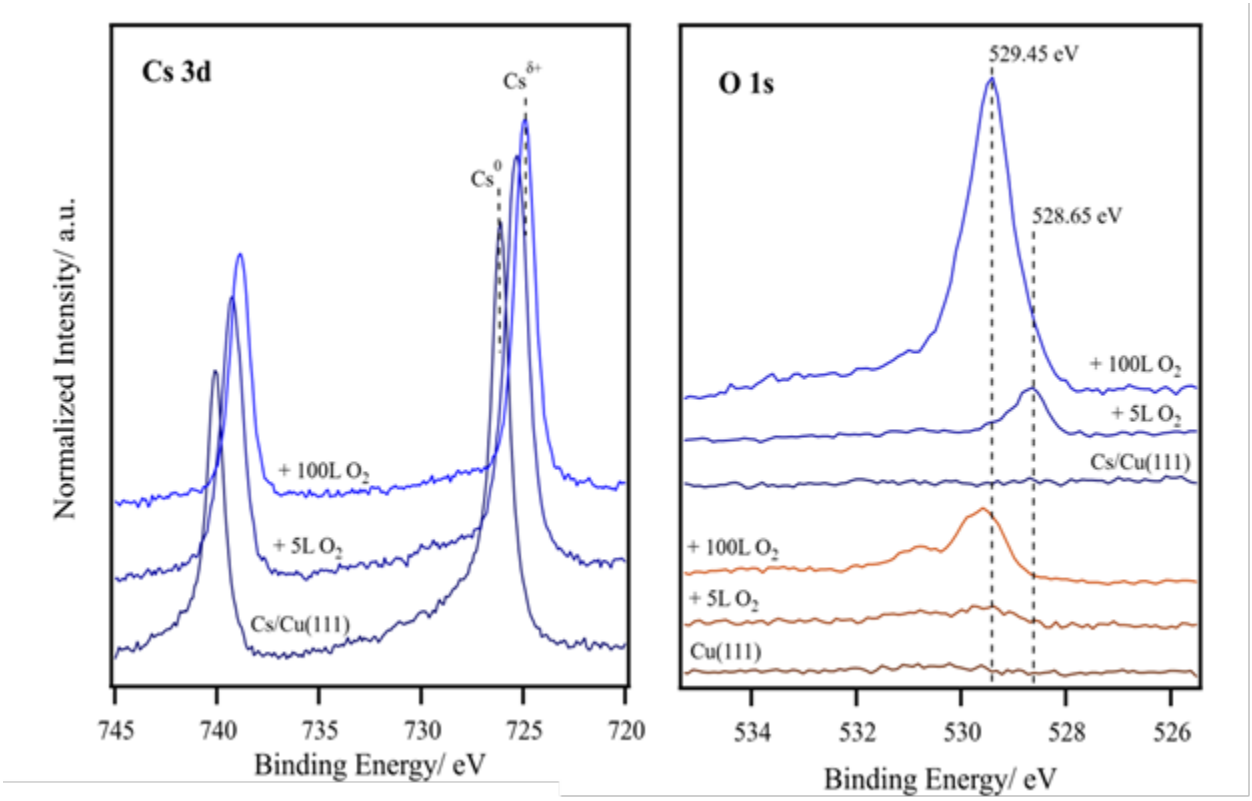

Figure 5: XPS spectra of oxidation of the Cs/Cu(111) surface. Cs coverage = 0.11 ML A) Cs 3d region shows a lower binding energy shift in Cs with addition of O_2. B) O 1s region shows the difference in oxidation for a cesiated and non-cesiated Cu surface. The bottom three orange spectra correspond to plain metallic copper before and after O_2 exposures of 5 and 100 L. The upper three blue spectra follow this oxidation with cesium on the Cu(111) surface. Spectrum intensity is normalized to the background.

The incorporation of alkalis on metallic surfaces is reported to have substantial effect on the adsorption kinetics of gases such as O_2.[19] Alkalis have allowed for the room temperature oxidation of notoriously inert surfaces such as Au(111).[63] More chemically active Fe(110) and Pt(111) have an O_2 sticking coefficient of 0.13 and 0.05, respectively. Incorporation of potassium on these surfaces brings this probability to near unity.[64,65] This effect is seen on Cu with Cs incorporation.[66]

Carley, et al., found that cesium on Cu(110) induced oxide structures only obtained by 4 orders of magnitude higher exposure on the bare Cu(110) facet.[67]

Kinetic experiments of oxygen uptake on Cu(111) surfaces show that the rate decreases with increasing temperature.[42] Wiame et al., concluded that this indicates a rate control mechanism of dissociative oxygen adsorption rather than via oxide nucleation site.[42] Alkali addition is believed to alter the adsorption characteristics of the catalyst surface via electron transfer and a lowered local work function.[19,64] In this way, it can be suggested that this creates a more favorable environment for the dissociation of oxygen to form partially oxidized alkali and substrate species. In a direct mechanism, the O_2 could dissociate over the alkali with the O adatoms spilling over to the copper surface. This phenomenon is consistent with the high reactivity of Cs and CsO_x towards O_2 and was previously postulated for the Cs-promoted oxidation of Zn films and Cu-Zn alloys.[68,69]

2. Cesium on Cu_2O/Cu(111)

2.1 Growth and chemical state of the alkali

We explored further Cs – Cu_xO interactions by preoxidizing the copper surface. We first grew an oxide film on the Cu(111), which is the '29' structure detailed in the literature.[44,70] This allows us to image the Cs as deposited onto the oxide thin film and obtain a better estimate of coverage in STM. We have investigated lower coverages of cesium that yield a range of 1-20% of the surface area. To our knowledge, this is the first study of cesium deposition on an oxide thin film. This may help us to understand the competition for oxygen between cesium and a transition metal oxide cation.

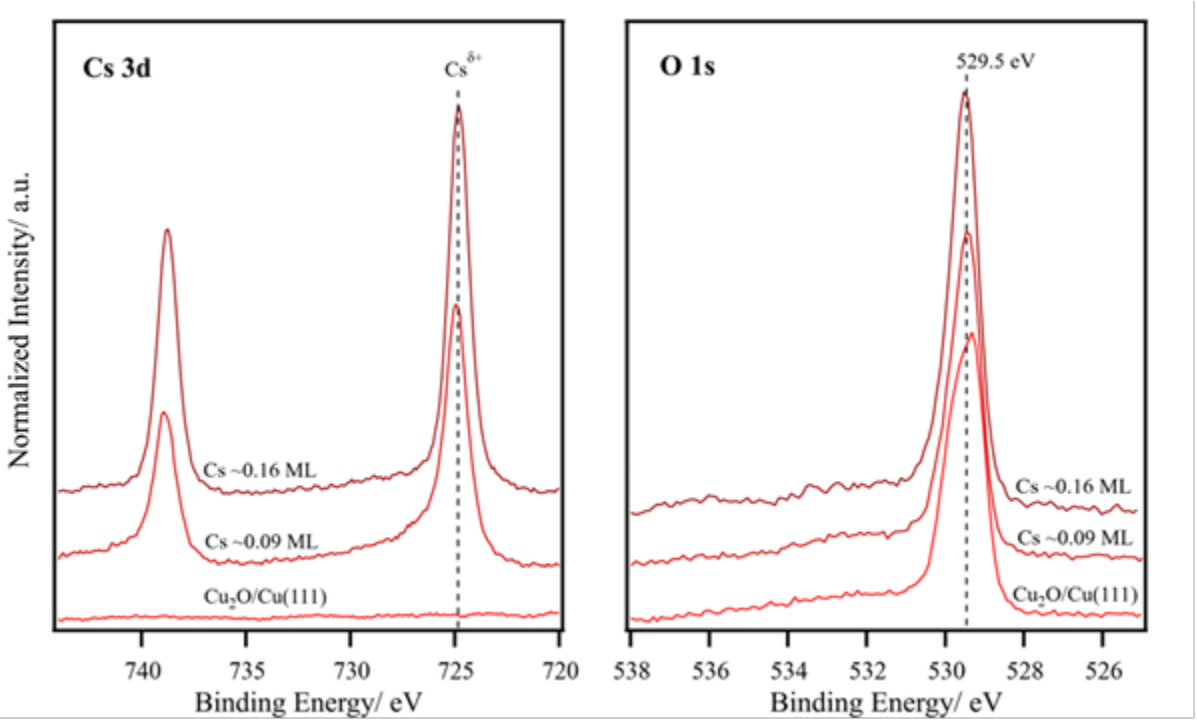

Figure 6: XPS spectra of the Cs 3d (left) and the O 1s (right) regions following two coverages of Cs deposited on Cu_2O/Cu(111). Deposition 1: 0.09 ML, Deposition 2: 0.16 ML. Spectrum intensity is normalized to the background.

XPS following two cesium depositions on the Cu_2O/Cu(111) surface are shown in figure 6. The Cs 3d peak intensities grow with each deposition and are oxidized at each coverage, with the 3d 5/2 peak centering on 724.8 eV. The plasmon features are largely absent from these spectra compared to those from cesium deposited onto the metallic surface (figure 1B). Their complementary spectra for the O 1s region are to the right, in which a sharpening of the primary peak at 529.5 eV occurs with Cs deposition, reminiscent of the oxidized cesiated surface seen in figure 4. Again, we conclude that this peak has multiple O-species contributions. From this, we infer that cesium sequestration of oxygen from the copper oxide thin film takes place upon deposition.

In corresponding STM images in figure 7, we observe the presence of cesium as a stable protrusion (1.5 – 2.2 Å high) on the thin oxide surface with lateral dimensions between 1.5 - 8 nm. There is no obvious shape preference. The Cs structures typically saturate the tunneling current, appearing as bright protrusions that are largely unresolvable. The distribution of cluster size would suggest multiple Cs atoms per cluster (the atomic radius of Cs is 2.98 Å). However, one assumes that

oxygen also makes up a part of these structures, as Cs recruits it from the oxide thin film as suggested from XPS above and seen in image 7B. The surrounding oxide thin film is riddled with point defects, which tend to be at higher density around the Cs structures. We find a trend toward further oxide structure breakdown surrounding these spots as more cesium is deposited onto the surface. This further supports the notion that cesium is sequestering oxygen from the oxide film and suggests an interplay between oxide affinity of the alkali and maintenance of the corrugated oxide structure.

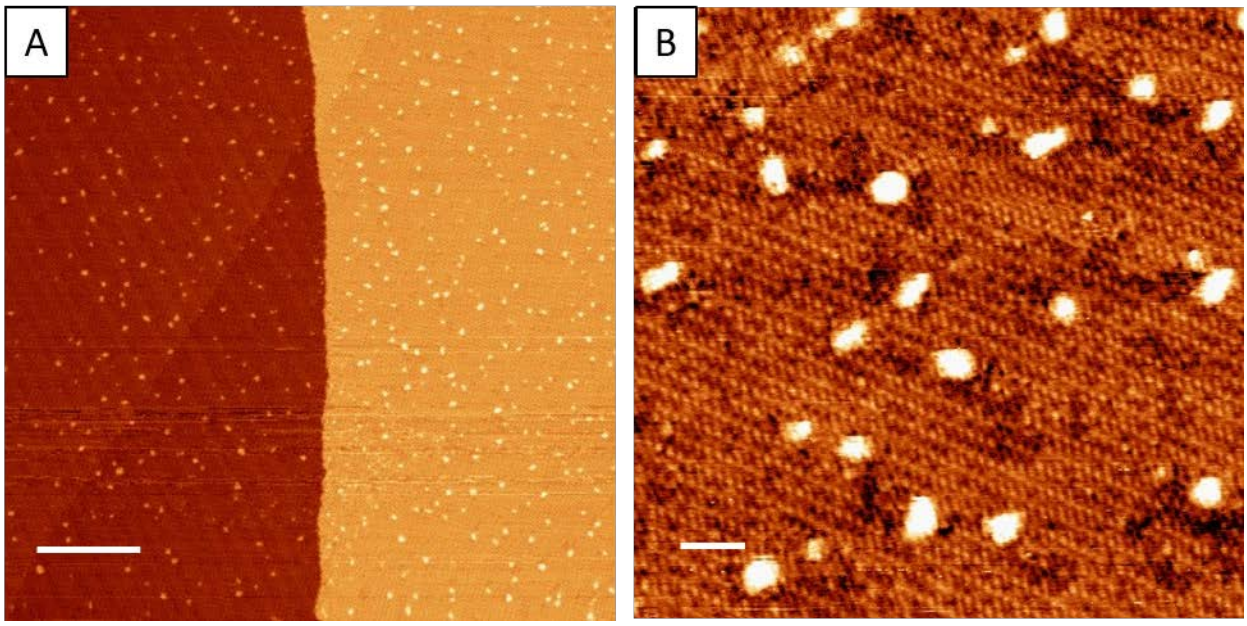

Figure 7: STM images of Cs on the Cu_2O film (10 s. deposition, ~0.04 MLE, V_t: 0.8 V, I_t: 0.1 nA). A) Large scale image showing uniform Cs dispersion on the surface. Scale Bar = 50 nm. B) Smaller scale image of the Cs structures on the Cu_2O film. Scale bar = 5.0 nm.

Increasing Cs deposition yields more protrusions as well as an increase in the range of size. S.I. figure S2 depicts this over 3 coverages of cesium on the Cu_2O/Cu(111) surface. An accompanying histogram shows the corresponding Cs cluster areas in square nm. The number and size range (in area) of the protrusions increase as the Cs coverage increases.

Due to the complexity in assignment of the atomic Cs-related features, and competing adsorbate systems over the Cu substrate, XPS spectra assist in the estimation of the coverage. We used both

the attenuation of the Cu 2p signal and the growth of Cs 3d to help determine coverages as described in the experimental section.

2.2 Resulting Surface Modifications and Mobility

STM experiments reveal a rich structural heterogeneity of the cesiated Cu_2O/Cu(111). The partial reduction of the oxide film took on some different morphologies, and resulting images were highly susceptible to the tip tunneling state. Most often at the coverages studied, the Cs structures induce a partial reduction of the oxide surface in the form of point defects as seen in figure 7B and figure 8 below. In figure 8, single point defects in the Cu_2O film structure dominate the breakdown. These sites are imaged with bright or dark contrast depending on the state of the tip (dark shown here), and likely consist of a loss of oxygen at the center of the oxide hexagon. Bright contrast defects stem from tunneling of Cu 3d states from the copper substrate.[42]

At times, the single point defects may organize into rows, as seen in figure 8. The dynamics of the reduced copper oxide thin film during the imaging process are notable in this image progression. In sequential scans (figure 8 A (time = 0s), B (time = 225s), C (t = 450s), D (t = 675s)) we can see that the defects of the thin film with Cs migrate over the surface, some forming defect rows. The mobility of the single point defects is much greater than those contained within the row structures. This extent of mobility does not seem to occur in the images of the non-cesiated surface, shown in supplemental figure S3.

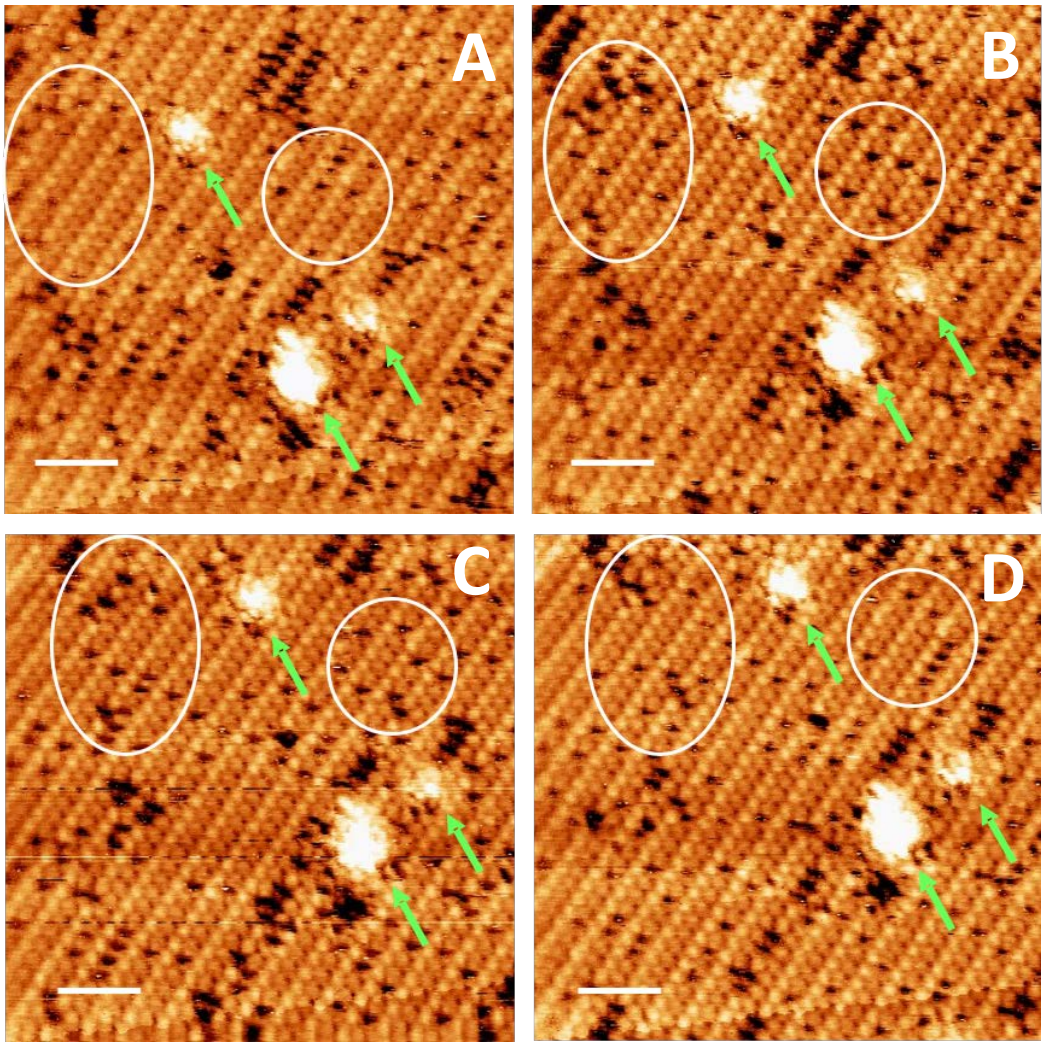

Figure 8: Sequential STM images of the Cs/Cu_xO/Cu(111) surface (A (time = 0s), B (time = 225s), C (t = 450s), D (t = 675s)), highlighting the oxide defect mobility. 30 nm^2, V_t: 1.3 V, I_t: 0.1 nA. Circles highlight areas where there is significant defect diffusion. Green arrows identify the Cs structures. Scale bars = 5.0 nm.

2.3 Thermal stability

The thermal stability of the Cs-Cu_2O/Cu(111) surface structure was followed through an annealing experiment. The resulting morphologies revolve around the formation and decay of an extended 'honeycomb'-like hexagonal superstructure (discussed below), which dominates the surface for much of the temperature range explored. Detailed STM images for each 50 K temperature

increment between 300 and 650 K are shown in S.I. figure S4. Figure 9 offers a summary of this transition of reproducible representative images.

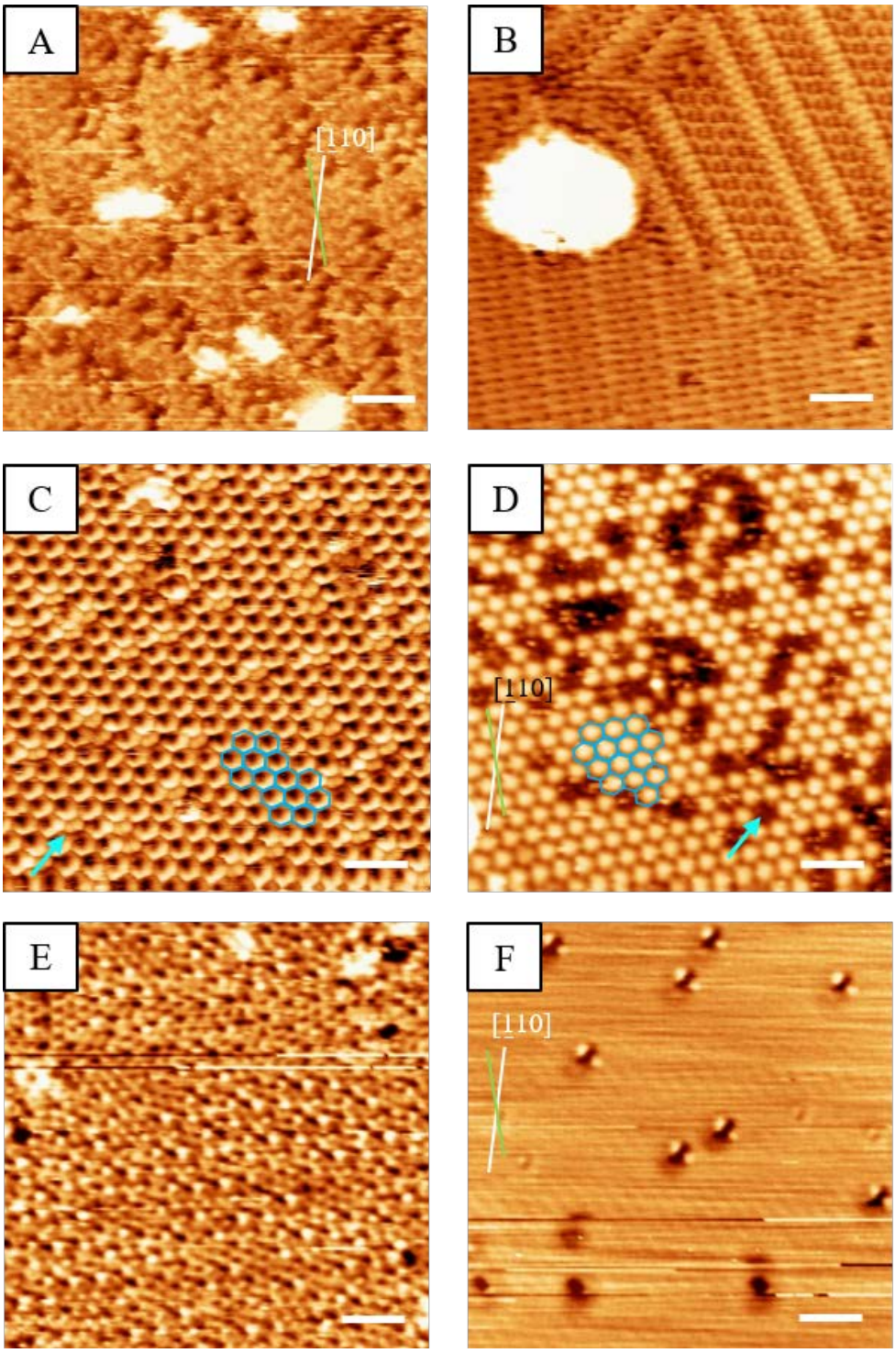

Figure 9: STM images of Cs-Cu_xO/Cu(111) over a progressive anneal (5 min each). All images are 20 nm^2, and scale bars = 3.0 nm. Imaging conditions are as follows: A) Cs as deposited on Cu_2O/Cu(111), 300 K, V_t: -1.1 V, I_t: -0.24 nA B) 350 K, V_t: -1.25 V, I_t: -0.23 nA C) 450 K, V_t: -1.13 V, I_t: -0.27 nA, D) 450 K, V_t: -1.25 V, I_t: -0.21 nA, E) 600 K, V_t: -1.05 V, I_t: -0.23 nA, F) 650 K, V_t: -1.25 V, I_t: II-0.24 nA.

Figure 9A is an image of Cs as-deposited on Cu_2O/Cu(111) at 300 K. A white line demarcates the [-110] family of directions of the Cu(111) surface, and the green line indicates the direction of the √13R46.1 side of the Cu_2O thin film lattice in Figure 9A, D and F. Morphological changes are immediately apparent upon annealing as seen in Figure 9B. Observations include the development of reduced domains within the corrugated Cu_2O thin film, which tend to take on the aforementioned honeycomb structure (highlighted in Figure 9C and D), and a slight growth in the diameter of the Cs structures (5 – 10 nm). This could be further mass transfer of oxygen from the oxide to the cesium clusters, and a restructuring of the clusters as they appear to take on some internal order. At 400 K, the corrugated Cu_2O structure is gone, giving way to the further formation of the flat hexagonal domains. Bright features that resemble fractured Cs protrusions are scattered about the surface. It is not until 450 K that the surface is relatively uniform with the flat honeycomb structure, as indicated by the blue hexagons in Figure 9C and D. This structure is maintained through 550 K (shown in S.I. fig. S4). As before, the contrast of the features largely depends on the tip tunneling state. This reconstruction occurs as either small symmetrical dot-like protrusions as in 9D or, qualitatively the opposite, as hexagons with a depression in the center where the dot would be located as in 9C. Defects are easily identified in this surface and are arranged in groups or occur as a single site. In 9D, these sites are dark areas where bright hexagonally packed dots are missing. The defects in 9C are indicated by smaller, brighter hexagons that seem to pull on the edges of their neighbors. A blue arrow points out these features on both images. The features here are all approximately 10 Å apart, just as those seen early in the oxidation of the Cs/Cu(111) surface, figure 4.

XPS in figure 10 shows that both Cs and O remain on the surface within this temperature range. To assist in the determination that cesium is contributing to the development of the honeycomb structure, we conducted a parallel annealing experiment of very low coverage (S.I. figure S5, ~0.02 MLE). This results in the same behavior, yet the honeycomb area does not extend over the long

range. Instead it is contained as domains amongst the corrugated Cu_2O thin film. Here we have evidence that this restructuring scales with cesium coverage, further suggesting that cesium makes up part of the structure.

Up to 500 K, the furthered development of the hexagonal 'honeycomb' feature with concomitant loss of Cs clusters and maintenance of Cs signal in XPS suggests that this is likely to be a pseudo-morphic structure of Cs, Cu and O. The 10 Å hexagonal spacing does not follow the dimensions of well-known copper oxide relaxations and breakdown structures. However, it does match the dimensions of the ordered structures formed by oxidation of Cs on metallic Cu(111) in Figure 4.

Further heating results in a breakdown of this extended ordered structure. At 600 K (Figure 9E), the honeycomb structure begins to break down. The surface is disordered over a long range, with bright dots that could be Cs atoms dispersed over domains of 6 Å-separated hexagons that resemble a partially reduced Cu_2O thin film. By 650 K, all remnants of the Cu_2O thin-film are gone (Figure 9F). This reduction occurs at lower temperatures than that of the Cu_2O surface alone.[43] The Cu(111) surface is decorated with a dark adsorbed species that appears to be a dimer or tetramer, as it contains two loci of electron density at opposite poles. It's appearance and size suggests something other than adsorbed atomic oxygen, which often appears on transition metals as a hole with rings of Friedel oscillations centered around the depression.[42] These surface species are stable through sequential scans and we have previously established that metallic Cs cannot be observed by STM on Cu(111) at room temperature. Figure 10 follows the O1s and Cs 3d spectra as the surface undergoes annealing through this range in temperature (blue to red). XPS indicates that neither Cs nor O are completely gone even up to 800 K, but the intensities decay significantly over the temperature range. This occurs mostly above 550 K, in keeping with conclusions from the STM images. As the cesium intensity decreases, the binding energy shifts up slightly from 724.7 eV, indicative of more metallic character, but does not transition completely to a neutral state. Thus, the surface species could exist as a cesium dimer complexed with the remaining oxygen. These features are also accompanied by significant streaking in the surrounding image, suggesting that highly mobile species are also present on the surface.

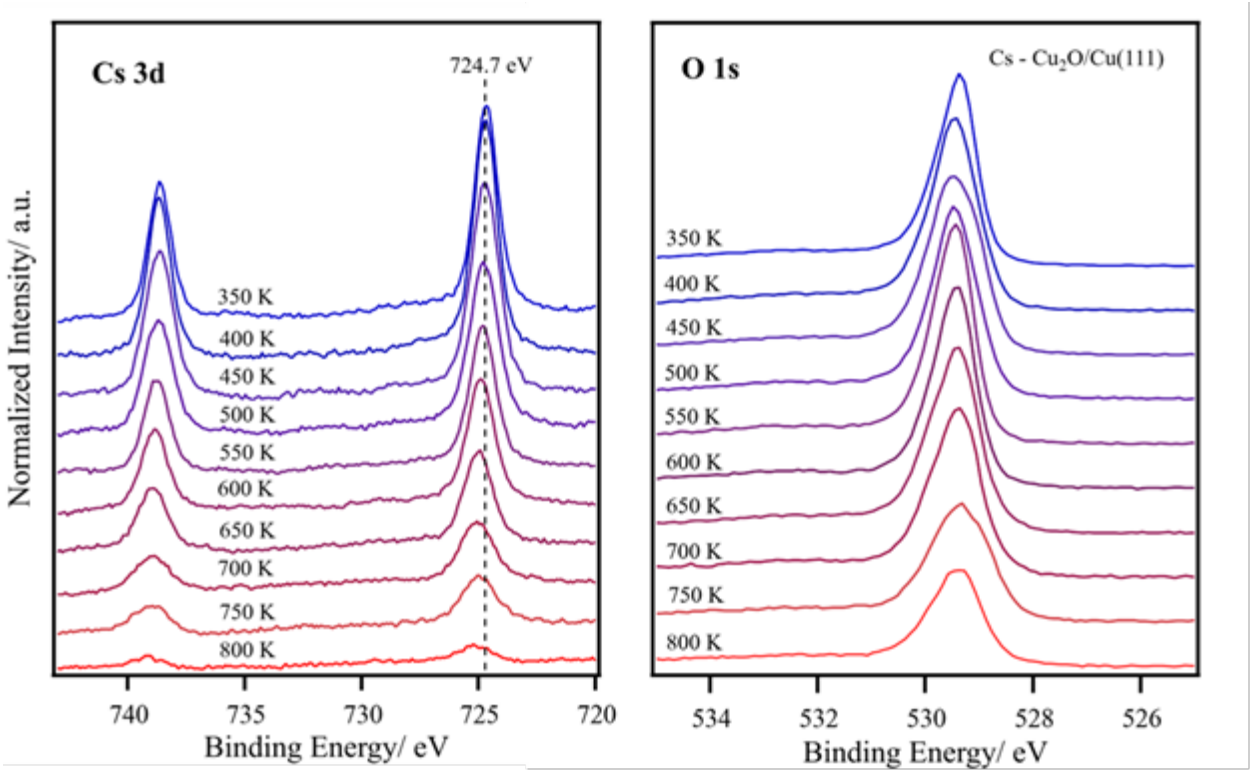

Figure 10: XPS spectra for the Cs 3d and O 1s regions of the Cs/Cu_xO/Cu(111) system during annealing. The initial cesium coverage was 0.09 ML. The temperature increases from blue (350 K) to red (800 K). Spectrum intensity is normalized to the background.

3. Theory

3.1. Density Functional Theory Calculations

We then explored the interaction of Cs on Cu_xO/Cu(111) which are shown in Figure 11. Here we have chosen $Cu_{1.1}O$/Cu(111) to describe the Cu_xO/Cu(111), detailed in a previous publication,[9] which accommodates some adsorbed oxygen in the center of the oxide rings. The DFT optimized structure of our $Cu_{1.1}O$/Cu(111) model is shown in Figure 11A, which consists of hexagonal substructures with partially filled oxygen (O_{ads}). Within the hexagonal ring the oxygen atoms adopt an alternate upper and lower position, following the approximate corrugation of the oxide thin film. In the DFT calculations, different adsorption sites on the $Cu_{1.1}O$/Cu(111) surface were considered for the nucleation of Cs: chemisorbed oxygen at the center of the hexagonal ring (O_{ads}), center of the hexagonal ring with no oxygen, three-coordinated upper oxygen atoms (O_U) and four-

coordinated lower oxygen atoms (O_L) as shown in Figure 11b-e, respectively. Unlike the case for metallic Cu(111), Cs adsorption on Cu_xO/Cu(111) shows strong preference for the adsorption site. The most stable adsorption site is directly over O_{ads} in the hexagonal ring with a BE of -3.29 eV, which is followed by the hexagonal ring with no oxygen (BE = -3.03 eV), O_L site (BE = -2.74 eV) and the O_U site (BE = -2.58 eV) in sequence. The bond distance between Cs and O_{ads} in the optimized structure (Figure 11b) is 2.98 Å. While the calculations do not lend themselves to mimicking the oxide breakdown seen in STM images as deposited, the adsorption of Cs in the hexagonal ring with or without the O_{ads} leads to slight distortion in the shape of the hexagonal structure (Figure 11b and c), as would be expected.

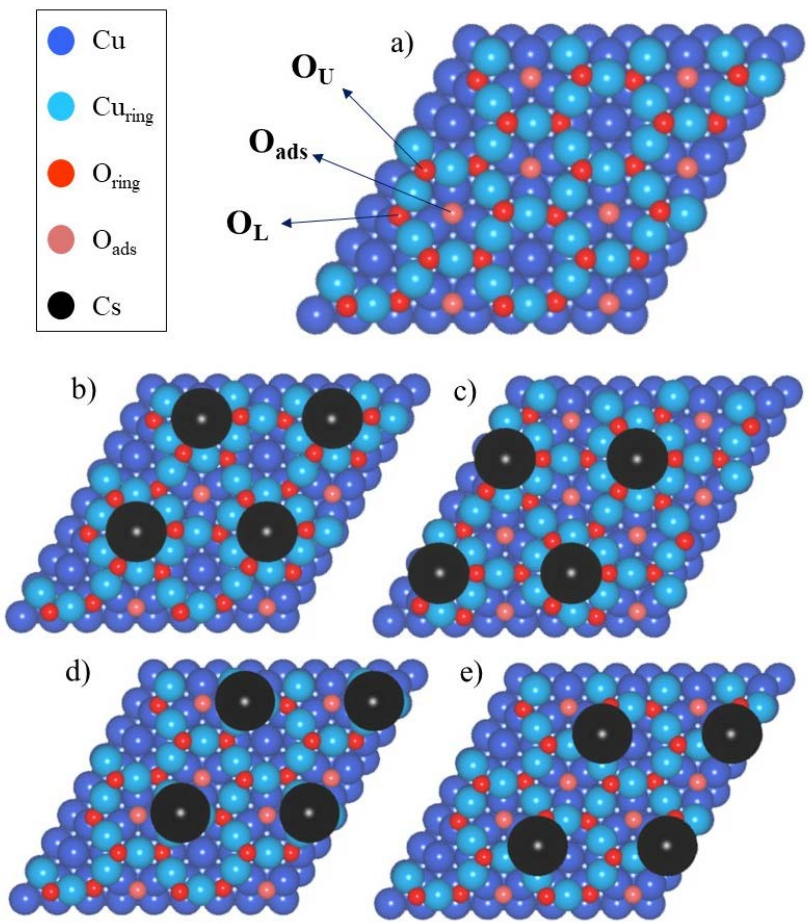

Figure 11: Cs adsorption on hex-$Cu_{1.1}O$ a) DFT optimized structure of $Cu_{1.1}O$ slab, Cs adsorption b) on O_{ads} site in the center of the hexagon, c) in the center of a copper oxide hexagon with no oxygen, d) on three coordinated O_U site, e) on four coordinated O_L site.

This coverage is lower than that of previous calculations of a related material surface of potassium on copper oxide thin films.[56] Where An and collaborators placed K in the center of each Cu_xO ring, here we have a significantly lower coverage around 0.06 ML (Cs_{atom}:Cu_{atom}) to more accurately reflect our data. The positions of the Cs atoms are such that the interatomic distance is 10.3 Å, which aligns with the features observed on the oxidized Cs on Cu(111) as well as the hexagonal 'honeycomb' structure seen in higher coverage or during annealing. It is likely that probing the cesium atoms would form the dot-like protrusion images, while tunneling to Cu or O states could form the 'honeycomb' hexagons. In theory, the areas where the Cs is missing, the dot protrusions are absent, and the hexagons are shrunken in, pulling nearby Cu_xO rings toward the defect center. While we cannot be certain that this is the final structure of the morphology described, its spacing, coverage and contrast features align very well. Based on this we propose that the DFT structure shown in Figure 11b represent the model for the hexagonal honeycomb structures observed in the STM images (Figure 9C). We suspect that this is the likely structure on this surface for many reactions under oxidizing conditions.

3.2. Electronic Interaction

Finally, to understand the electronic interaction, we have calculated the pseudo difference of the electronic charge density ($\Delta\rho$) for Cs adsorption on Cu(111) and Cu_xO/Cu(111) surfaces. $\Delta\rho$ is calculated by using the formula:

$$\Delta\rho = \rho_{Cs/slab} - (\rho_{slab} + \rho_{Cs})$$

Where $\rho_{Cs/slab}$ is the total electronic charge density when Cs is adsorbed on Cu(111) or Cu_xO/Cu(111) surfaces. ρ_{slab} corresponds to the charge density of the Cu(111) or Cu_xO/Cu(111) slabs and ρ_{Cs} corresponds to that of the Cs atom. Figure 12 a and b shows the charge density difference plot for Cs adsorption on the Cu(111) atop site. Upon adsorption, a depletion of charge density was observed around Cs with charge accumulation observed over every Cu(111) surface atom. This indicates ionic bonding between Cs and Cu as observed in previous experimental study.[28,35] Figure 12 c and d show the charge density difference plots for Cs adsorption on the O_{ads} site of the Cu_xO/Cu(111) substrate (introduced in Figure 11b), which is energetically the most

stable structure and models our STM observation. The CDD plots show an accumulation of charge density around surface Cu and O atoms and a depletion of charge around the Cs atom similar to Cu(111). However, the accumulation of charge density lobes is greater on the Cu_xO/Cu(111) system than for Cu(111), which agrees with the stronger adsorption energy of Cs on Cu_xO/Cu(111) than for Cu(111) systems. Further, the greater polarization and anisotropic effects of the charge density difference on the Cu_xO/Cu(111) surface exemplify how the oxide structure serves to anchor the cesium atoms from high surface mobility.

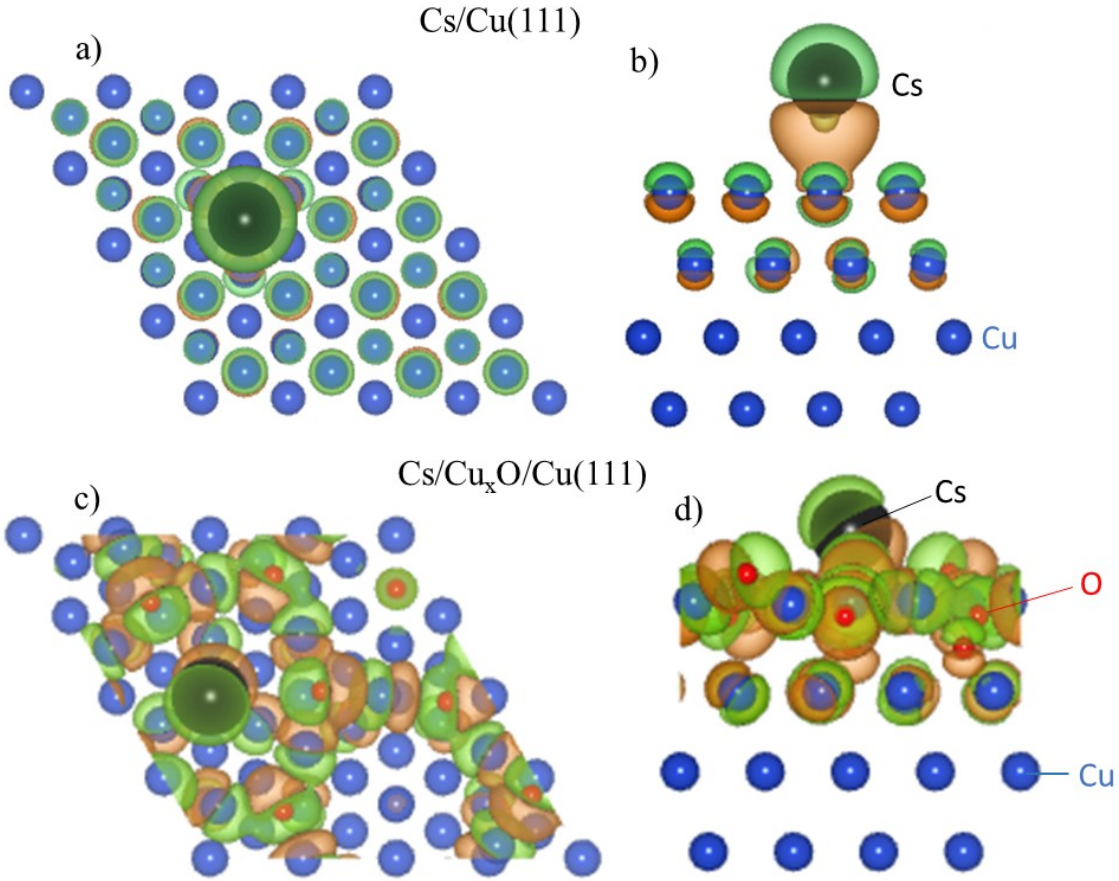

Figure 12: Calculated charge density difference (CDD) for a,b) Cs adsorbed on Cu(111) atop site and c,d) Cs adsorbed on Cu_xO/Cu(111) on the O_{ads} site. Perspectives include: a,c) top view b,d) side view. The isosurface level was chosen as 0.01 e $Å^{-3}$. Contours indicate the electron density increase (green) or decrease (orange) by 0.01 e $Å^{-3}$. Color representation: blue = Cu, black = Cs, Red = O.

CONCLUSIONS

In this work we have investigated the surface morphology and chemical state of Cs on Cu(111) under pre and post-oxidation conditions. On the metallic surface, we have confirmed earlier reports of high surface mobility of Cs on fcc facets such as Cu(111). This is further verified by DFT calculations which show that Cs does not have a preferential absorption site on Cu(111) which may lead to high surface mobility. The alkali is clearly on the surface as shown in XPS, which also indicates that the species is slightly cationic at low coverages with more metallic character as coverage increases. Oxidation of this Cs pre-covered surface occurs more readily than on the unmodified surface and implies that cesium may promote the dissociation and oxidation of the surface. In STM we can see development of a hexagonal surface structure of 9-10 Å that is not known to just copper and oxygen forming on the terraces.

Cesium deposited onto a Cu_2O/Cu(111) surface results in stable, protruding clusters on the surface that scale with the deposition time, often with accompanying partial breakdown of the Cu_2O thin film. This breakdown exhibits a complex and varied morphology. General trends include mobile point defects in the Cu_2O, which at times may arrange into lines as well as flat, close-packed hexagonal structures which tend to form with further disruption to the corrugated oxide. The surface structure is highly sensitive to temperature. While higher coverage of Cs alone can induce the formation of the hexagonal 10 Å 'honeycomb' structure, a mild departure from room temperature will also induce this formation for all coverages. Our DFT calculations provide an atomic scale model for the observed hexagonal honeycomb structure in STM. It seems that any disruption to the Cu_2O structure facilitates the formation of this honeycomb morphology, be it through higher coverages, proximity to step edges, or with elevated temperature. Eventually this structure breaks down at higher temperatures ($\geq$600 K) to yield oxidized cesium clusters on the metallic copper substrate. We anticipate that the 'honeycomb' structure on this surface may be the likely morphology for many reactions at lower temperatures or oxidative potential, and the oxidized Cs clusters on Cu(111) may be the active form for reactions at higher temperatures or reductive potential.

ACKNOWLEDGMENT

The research carried out at Brookhaven National Laboratory, was supported by the U.S. Department of Energy (DOE), Office of Science and Office of Basic Energy Sciences under contract No. DE-SC0012704. This work utilized instrumentation and computational resources of the Center for Functional Nanomaterials and the 23-ID-2 (IOS) beamline at the National Synchrotron Light Source II (IOS), which are DOE Office of Science User Facilities also under Contract No. DE-SC0012704. SDS is partially supported by a U.S. DOE Early Career Award.

REFERENCES

(1) Campbell, C. T.; Koel, B. E. A Model Study of Alkali Promotion of Water-Gas Shift Catalysts: Cs/Cu(111). *Surf. Sci.* **1987**, *186*, 393–411.

(2) Klier, K.; Young, C.-W.; Nunan, J. G. Promotion of the Water Gas Shift Reaction by Cesium Surface Doping of the Model Binary Cu/ZnO Catalyst. *Ind. Eng. Chem. Fundam. Appl. Catal.* **1986**, *25* (77), 36–42.

(3) Nunan, J.; Klier, K.; Young, C.-W.; Himelfarb, P. 6; Herman, R. G. Promotion of Methanol Synthesis over Cu/ZnO Catalysts by Doping with Caesium. *J. Chem. Soc., Chem. Commun.* **1986**, 193–195.

(4) Aika, K.; Hori, H.; Ozaki, A. Activation of Nitrogen by Alkali Metal Promoted Transition Metal I. Ammonia Synthesis over Ruthenium Promoted by Alkali Metal. *J. Catal.* **1972**, *27* (3), 424–431.

(5) Cowell, J. J.; Santra, A. K.; Lambert, R. M. Ultraselective Epoxidation of Butadiene on Cu(111) and the Effects of Cs Promotion. *J. Am. Chem. Soc* **2000**, *122*, 2381–2382.

(6) McClory, M. M.; Gonzalez, R. D. The Role of Alkali Metals as Promoters in the Methanation and Fischer-Tropsch Reaction: An *in Situ* Study. *J. Catal.* **1984**, *89* (2), 392–403.

(7) Petala, A.; Panagiotopoulou, P. Methanation of CO_2 Over Alkali-Promoted Ru/TiO_2 Catalysts: I. Effect of Alkali Additives on Catalytic Activity and Selectivity. *Appl. Catal.*

B Environ. **2018**, *224*, 919–927.

(8) Ahlers, S. J.; Pohl, M.-M.; Radnik, J.; Linke, D.; Kondratenko, E. V. Catalytic Role and Location of Cs Promoter in Cs–Au/TiO_2 Catalysts for Propanol Synthesis from CO_2, C_2H_4 and H_2. *Appl. Catal. B Environ.* **2015**, *176*, 570–577.

(9) Ahlers, S. J.; Pohl, M.-M.; Holena, M.; Linke, D.; Kondratenko, E. V. Direct Propanol Synthesis from CO_2, C_2H_4, and H_2 over Cs–Au/TiO_2 Rutile: Effect of Promoter Loading, Temperature and Feed Composition. *Catal. Sci. Technol.* **2016**, *6* (7), 2171–2180.

(10) Shi, Z.; Yang, H.; Gao, P.; Chen, X.; Liu, H.; Zhong, L.; Wang, H.; Wei, W.; Sun, Y. Effect of Alkali Metals on the Performance of CoCu/TiO_2 Catalysts for CO_2 Hydrogenation to Long-Chain Hydrocarbons. *Chinese J. Catal.* **2018**, *39* (8), 1294–1302.

(11) Diehl, R. D.; Mcgrath, R. Structural Studies of Alkali Metal Adsorption and Coadsorption on Metal Surfaces. *Surf. Sci. Rep.* **1996**, *23*, 43–171.

(12) Lindgren, S. Å.; Walldén, L.; Hedin, L. Structure and Electronic Properties of Cs Adsorbed on Cu(111). *Solid State Commun.* **1978**, *25*, 13–15.

(13) Campbell, C. T. Cesium-Promoted Silver(111): Model Studies of Selective Ethylene Oxidation Catalysts. *J. Phys. Chem.* **1985**, *89* (26), 5789–5795.

(14) Ziegler, M.; Kröger, J.; Berndt, R.; Filinov, A.; Bonitz, M. Scanning Tunneling Microscopy and Kinetic Monte Carlo Investigation of Cesium Superlattices on Ag(111).

(15) Grant, R. B.; Lambert, R. M. Alkali Metal Promoters and Catalysts: A Single-Crystal Investigation of Ethylene Epoxidation on Cesium-Doped Silver(111). *Langmuir* **1985**, *1* (1), 29–33.

(16) Jacobi, K.; Shi, H.; Dietrich, H.; Ertl, G. Adsorbate-Induced Electronic Modification of Cs Overlayers on Ru(0001). *Surf. Sci.* **1995**, 69–74.

(17) Sham, T. K.; Shek, M.-L.; Hrbek, J. Coverage Dependent Core-Level Shifts of Cs Adsorbed on Ru(001) and Observation of Surface Defects with a Cs Probe. *Surf. Sci. Lett.* **1991**, *241*, L16–L20.

(18) Ayyoob, M.; Hegde, M. S. An XPS Study of the Adsorption of Oxygen on Silver and

Platinum Surfaces Covered with Potassium or Cesium. *Surf. Sci.* **1983**, *133*, 516–532.

(19) Bonzel, H. P. Alkali-Metal-Affected Adsorption of Molecules on Metal Surfaces. *Surf. Sci. Rep.* **1988**, *8* (2), 43–125.

(20) Langmuir, I.; Villars, D. S. Oxygen Films on Tungsten. I. A Study of Stability by Means of Electron Emission in Presence of Cesium Vapor. *J. Am. Chem. Soc.* **1931**, *53* (2), 486–497.

(21) Gerlach, R. L.; Rhodin, T. N. Binding and Charge Transfer Associated with Alkali Metal Adsorption on Single Crystal Nickel Surfaces. *Surf. Sci.* **1970**, *19* (2), 403–426.

(22) Madey, T. E.; Yakshinskiy, B. V; Ageev, V. N.; Johnson, R. E. Desorption of Alkali Atoms and Ions from Oxide Surfaces: Relevance to Origins of Na and K in Atmospheres of Mercury and the Moon. *J. Geophys. Res.* **1998**, *103* (E3).

(23) Noguera, C.; Bordier, G. Theoretical Approach to Interfacial Metal-Oxide Bonding. *J. Phys. III* **1994**, *4* (10), 1851–1864.

(24) Grant, A. W.; Campbell, C. T. Cesium Adsorption on TiO_2(110). *Phys. Rev. B* **1997**, *55* (3), 1844–1851.

(25) Brause, M.; Skordas, S.; Kempter, V. Study of the Electronic Structure of TiO_2(110) and Cs/TiO_2(110) with Metastable Impact Electron Spectroscopy and Ultraviolet Photoemission Spectroscopy (HeI). *Surf. Sci.* **2000**, *445*, 224–234.

(26) Vedage, G. A.; Himelfarb, P. B.; Simmons, G. W.; Klier, K. Alkali-Promoted Copper-Zinc Oxide Catalysts for Low Alcohol Synthesis. *ACS Symp. Ser.* **1985**, *279*, 295–312.

(27) Campos-Martín, J. M.; Fierro, J. L. G.; Guerrero-Ruiz, A.; Herman, R. G.; Klier, K. Promoter Effect of Cesium on C–C Bond Formation during Alcohol Synthesis from CO/H_2 over Cu/ZnO/Cr_2O_3 Catalysts. *J. Catal.* **1996**, *163*, 418–428.

(28) Lindgren, S. Å. A.; Walldén, L. Cu Surface State and Cs Valence Electrons in Photoelectron Spectra from the Cu(111)/Cs Adsorption System. *Solid State Commun.* **1978**, *28* (3), 283–286.

(29) Lindgren, S. Å.; Wallden, L. Dilution of the Electron Gas in a Cesium Monolayer on

Copper(111) by Adsorption of Oxygen. *Surf. Sci.* **1979**, *80*, 620–625.

(30) Rodriguez, J. A.; Clendening, W. D.; Campbell, C. T. Adsorption of CO and CO_2, on Clean and Cesium-Covered Cu(110). *J . Phys. Chem* **1989**, *93*, 5238–5248.

(31) Lindgren, S. Å.; Wallden, L.; Rundgren, J.; Westrin, P.; Neve, J. Structure of Cu(111)p(2x2)Cs Determined by Low-Energy Electron Diffraction. *Phys. Rev. B* **1983**, *28* (12).

(32) Lindgren, S. Å.; Wallden, L. Electronic Structure of Clean and Oxygen-Exposed Na and Cs Monolayers on Cu(111). *Phys. Rev. B* **1980**, *22* (12).

(33) Carley, A. F.; Roberts, M. W.; Strutt, A. J. Activation of Carbon Monoxide and Carbon Dioxide at Cesium-Promoted Cu(110) and Cu(110)-O Surfaces. *J. Phys. Chem.* **1994**, *98* (37), 9175–9181.

(34) Lindgren, S. Å.; Wallden, L. Layer-by-Atomic-Layer Desorption of Cs from Cu(111)/Cs Observed via Photoemission. *J. Phys. Condens. Matter* **1990**, *2* (26), 5929–5932.

(35) Lindgren, S. Å.; Walldén, L. Energy Shifts of a Cu(111) Surface Band upon Adsorption of Cesium and Oxygen. *Surf. Sci.* **1979**, *89* (1–3), 319–326.

(36) Fan, W. C.; Ignatiev, A. Ordered Phases and Phase Transitions of Cesium on the Cu(111) Surface. *Cit. J. Vac. Sci. Technol. A* **1988**, *6*, 735.

(37) Von Hofe, T.; Kröger, J.; Berndt, R. Adsorption Geometry of Cu(111)-Cs Studied by Scanning Tunneling Microscopy. *Phys. Rev. B - Condens. Matter Mater. Phys.* **2006**, *73* (24), 1–7.

(38) Regoutz, A.; Kerherve, G.; Villar-Garcia, I.; Williams, C. K.; Payne, D. J. The Influence of Oxygen on the Surface Interaction between CO_2 and Copper Studied by Ambient Pressure X-Ray Photoelectron Spectroscopy. *Surf. Sci.* **2018**, *677*, 121–127.

(39) Clendening, W. D.; Rodriguez, J. A.; Campbell, J. M.; Campbell, C. T. The Chemisorption and Coadsorption of Water and Oxygen on Cs-Dosed Cu(110). *Surf. Sci.* **1989**, *216*, 429–461.

(40) Henn, F. C.; Rodriguez, J. A.; Campbell, C. T. Adsorption and Reaction of HCOOH on

Doped Cu(110): Coadsorption with Cesium, Oxygen, and $Cs_a + O_A$. *Surf. Sci.* **1990**, *236* (3), 282–312.

(41) Baber, A. E.; Yang, X.; Kim, H. Y.; Mudiyanselage, K.; Soldemo, M.; Weissenrieder, J.; Senanayake, S. D.; Al-Mahboob, A.; Sadowski, J. T.; Evans, J.; et al. Stabilization of Catalytically Active Cu^+ Surface Sites on Titanium-Copper Mixed-Oxide Films. *Angew. Chemie Int. Ed.* **2014**, *53* (21), 5336–5340.

(42) Wiame, F.; Maurice, V.; Marcus, P. Initial Stages of Oxidation of Cu(111). *Surf. Sci.* **2007**, *601*, 1193–1204.

(43) Matsumoto, T.; Bennett, R. a. A.; Stone, P.; Yamada, T.; Domen, K.; Bowker, M. Scanning Tunneling Microscopy Studies of Oxygen Adsorption on Cu(111). *Surf. Sci.* **2001**, *471*, 225–245.

(44) Therrien, A. J.; Zhang, R.; Lucci, F. R.; Marcinkowski, M. D.; Hensley, A.; Mcewen, J.-S.; Charles Sykes, E. H. Structurally Accurate Model for the “29”-Structure of CuxO/Cu(111): A DFT and STM Study. *J . Phys. Chem. C* **2016**.

(45) Horcas, I.; Fernández, R.; Gómez-Rodríguez, J. M.; Colchero, J.; Gómez-Herrero, J.; Baro, A. M. WSXM: A Software for Scanning Probe Microscopy and a Tool for Nanotechnology. *J. Appl. Phys. Rev. Sci. Instruments* **2007**, *78* (82), 13705–71101.

(46) Palomino, R. M.; Stavitski, E.; Waluyo, I.; Karen Chen-Wiegart, Y.; Abeykoon, M.; Sadowski, J. T.; Rodriguez, J. A.; Frenkel, A. I.; Senanayake, S. D. New *in-Situ* and Operando Facilities for Catalysis Science at NSLS-II: The Deployment of Real-Time, Chemical, and Structure-Sensitive X-Ray Probes. *Synchrotron Radiat. News* **2017**, *30* (2), 30–37.

(47) Seah, M.; Dench, W. Quantitative Electron Spectroscopy of Surfaces: A Standard Data Base for Electron Inelastic Mean Free Paths in Solids. *Surf. Interface Anal.* **1979**, *1* (1), 46–55.

(48) Jablonski, A.; Zemek, J. Overlayer Thickness Determination by XPS Using the Multiline Approach. *Surf. Interface Anal.* **2008**, *41*, 193–204.

(49) Blöchl, P. E. Projector Augmented-Wave Method. *Phys. Rev. B* **1994**, *50* (24), 17953–

17979.

(50) Kresse, G.; Joubert, D. From Ultrasoft Pseudopotentials to the Projector Augmented-Wave Method. *Phys. Rev. B* **1999**, *59* (3), 1758–1775.

(51) Kresse, G.; Furthmüller, J. Efficient Iterative Schemes for Ab Initio Total-Energy Calculations Using a Plane-Wave Basis Set. *Phys. Rev. B* **1996**, *54* (16), 11169–11186.

(52) Kresse Av, G.; Furthmiiller, J. Efficiency of Ab-Initio Total Energy Calculations for Metals and Semiconductors Using a Plane-Wave Basis Set. *Comput. Mater. Sci.* **1996**, *6*, 15–50.

(53) Kresse, G.; Hafner, J. Ab Initio Molecular Dynamics for Liquid Metals. *Phys. Rev. B* **1993**, *47* (1), 558–561.

(54) Perdew, J. P.; Chevary, J. A.; Vosko, S. H.; Jackson, K. A.; Pederson, M. R.; Singh, D. J.; Fiolhais, C. Erratum: Atoms, Molecules, Solids, and Surfaces: Applications of the Generalized Gradient Approximation for Exchange and Correlation. *Phys. Rev. B* **1993**, *48* (7), 4978–4978.

(55) Monkhorst, H. J.; Pack, J. D. Special Points for Brillouin-Zone Integrations. *Phys. Rev. B* **1976**, *13* (12), 5188–5192.

(56) An, W.; Xu, F.; Stacchiola, D.; Liu, P. Potassium-Induced Effect on the Structure and Chemical Activity of the Cu_xO/Cu(111) (X≤2) Surface: A Combined Scanning Tunneling Microscopy and Density Functional Theory Study. *Chem. Cat. Chem.* **2015**, *7* (23), 3865–3872.

(57) Neugebauer, J.; Scheffler, M. Adsorbate-Substrate and Adsorbate-Adsorbate Interactions of Na and K Adlayers on Al(111). *Phys. Rev. B* **1992**, *46* (24), 16067–16080.

(58) Mcdonnell, L.; Woodruff, D. P. A LEED Study of Oxygen Adsorption on Copper(100) and (111) Surfaces. *Surf. Sci.* **1974**, *46*, 505–536.

(59) Dubois, L. H. Oxygen Chemisorption and Cuprous Oxide Formation on Cu(111): A High Resolution EELS Study. *Surf. Sci.* **1982**, *119* (2–3), 399–410.

(60) Spitzer, A.; Lüth, H. The Adsorption of Oxygen on Copper Surfaces: II. Cu(111). *Surf.*

Sci. **1982**, *118* (1–2), 136–144.

(61) Lindgren, S. Å.; Wallḑen, L. Oxygen Adsorption Induced Energy Shift of a Surface State on Cesium Covered Cu(111). *Chem. Phys. Lett.* **1979**.

(62) Hwang, C. C.; An, K. S.; Park, R. J.; Kim, J. S.; Lee, J. B.; Park, C. Y.; Lee, S. B.; Kimura, A.; Kakizaki, A. Cesium Core Level Binding Energy Shifts at the O_2/Cs/Si(113) Surface. *J. Electron Spectros. Relat. Phenomena* **1998**, *88*, 91–733.

(63) Ren, J.; Wang, Y.; Zhao, J.; Tan, S.; Petek, H. K Atom Promotion of O_2 Chemisorption on Au(111) Surface. *J. Am. Chem. Soc* **2019**, *141*, 39.

(64) Pirug, G.; Bonzel, H. P.; Brodén, G. The Adsorption of Potassium on Pt(111) and Its Effect on Oxygen Adsorption. *Surf. Sci.* **1982**, *122* (1), 1–20.

(65) Bonzel, H. P.; Ku, R. On the Kinetics of Oxygen Adsorption on a Pt(111) Surface. *Surf. Sci.* **1973**, *40*, 85–101.

(66) Habraken, F. H. P. M.; Kieffer, E. P.; Bootsma, G. A. A Study of the Kinetics of the Interactions of O_2 and N_2O with a Cu(111) Surface and of the Reaction of CO with Adsorbed Oxygen Using AES, LEED and Ellipsometry. *Surf. Sci.* **1979**, *83* (1), 45–59.

(67) Carley, A. F.; Davies, P. R.; Harikumar, K. R.; Jones, R. V.; Roberts, M. W. Reactivity and Structural Aspects of Cesium and Oxygen States at Cu(110) Surfaces: An XPS and STM Investigation. *J. Phys. Chem. B* **2004**, *108* (38), 14518–14526.

(68) Hrbek, J.; Yang, Y. W.; Rodriguez, J. A. Oxidation of Cesium Multilayers. *Surf. Sci.* **1993**, *296*, 164–170.

(69) Chaturvedi, S.; Rodriguez, J.; Hrbek, J. Cs Promoted Oxidation of Zn and Cu-Zn Surfaces: A Combined Experimental and Theoretical Study. *Surf. Sci.* **1997**, *384*, 260

(70) Jensen, F.; Besenbacher, F.; Laegsgaard, E.; Stensgaard, I. Oxidation of Cu(111): Two New Oxygen Induced Reconstructions. *Surf. Sci. Lett.* **1991**, *259*, L774–L780.

TOC

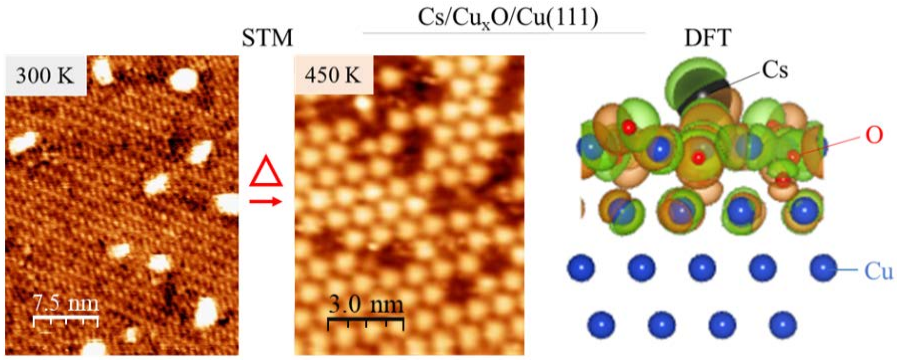

Supplemental Information: Structural and Chemical State of Cesium on Well-Defined Cu(111) and Cu_2O/Cu(111) Surfaces

Rebecca C. E. Hamlyn[1], Mausumi Mahapatra,[2] Ivan Orozco,[1] Ira Waluyo,[3] Adrian Hunt,[3] José A. Rodriguez,[1,2] Michael G.White,[1,2,*] and Sanjaya D. Senanayake, [2,*]

[1] Chemistry Department, Stony Brook University, Stony Brook, NY 11794 USA

[2] Chemistry Department, Brookhaven National Laboratory, Upton, NY 11973 USA

[3] National Synchrotron Light Source II, Brookhaven National Laboratory, Upton, NY 11973 USA

Corresponding Authors: * SDS, ssnanay@bnl.gov; MGW, mgwhite@bnl.gov; Bldg. 555A, Brookhaven National Laboratory, P.O. Box 5000, Upton, NY 11973-5000

1) Oxidized CsO_x structures on Cu(111)

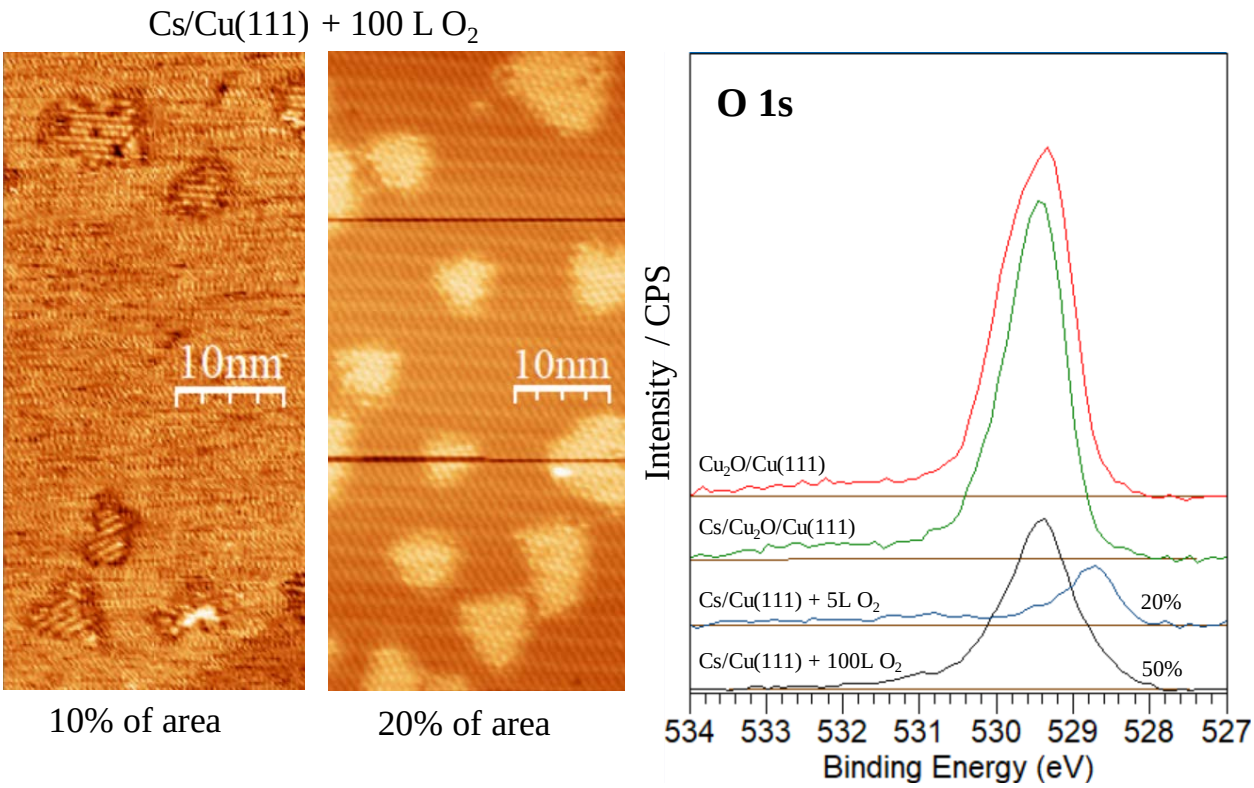

Figure S1. Left: STM images for 2 coverages of Cs on Cu(111) exposed to approximately 100 L O_2, demonstrating the linear scaling relationship of the hexagonal array formation to the Cs coverage. The coverage on the right is twice the coverage on the left, and the areas of the hexagonally ordered arrays are about 10% and 20%, respectively. Any differences in contrast are simply due to changes in the tip. Left: V_t: -1.2 V, I_t: 0.1 nA. Right: V_t: -1.14 V, I_t: 0.1 nA.

Right: XPS spectra comparing O 1s regions for different surface preparations. The first two spectra correspond to the fully oxidized Cu(111) surface (red), and then a 10 second Cs deposition on top of this (green). These areas are essentially unity. When the same dose of Cs is deposited onto metallic Cu(111) and exposed to O_2, the peak areas correspond to ~20% at 5 L and ~50% at 100 L of the fully oxidized intensity. This supports the theory of some oxygen spillover from Cs onto Cu(111).

2) Cs/Cu_2O coverage

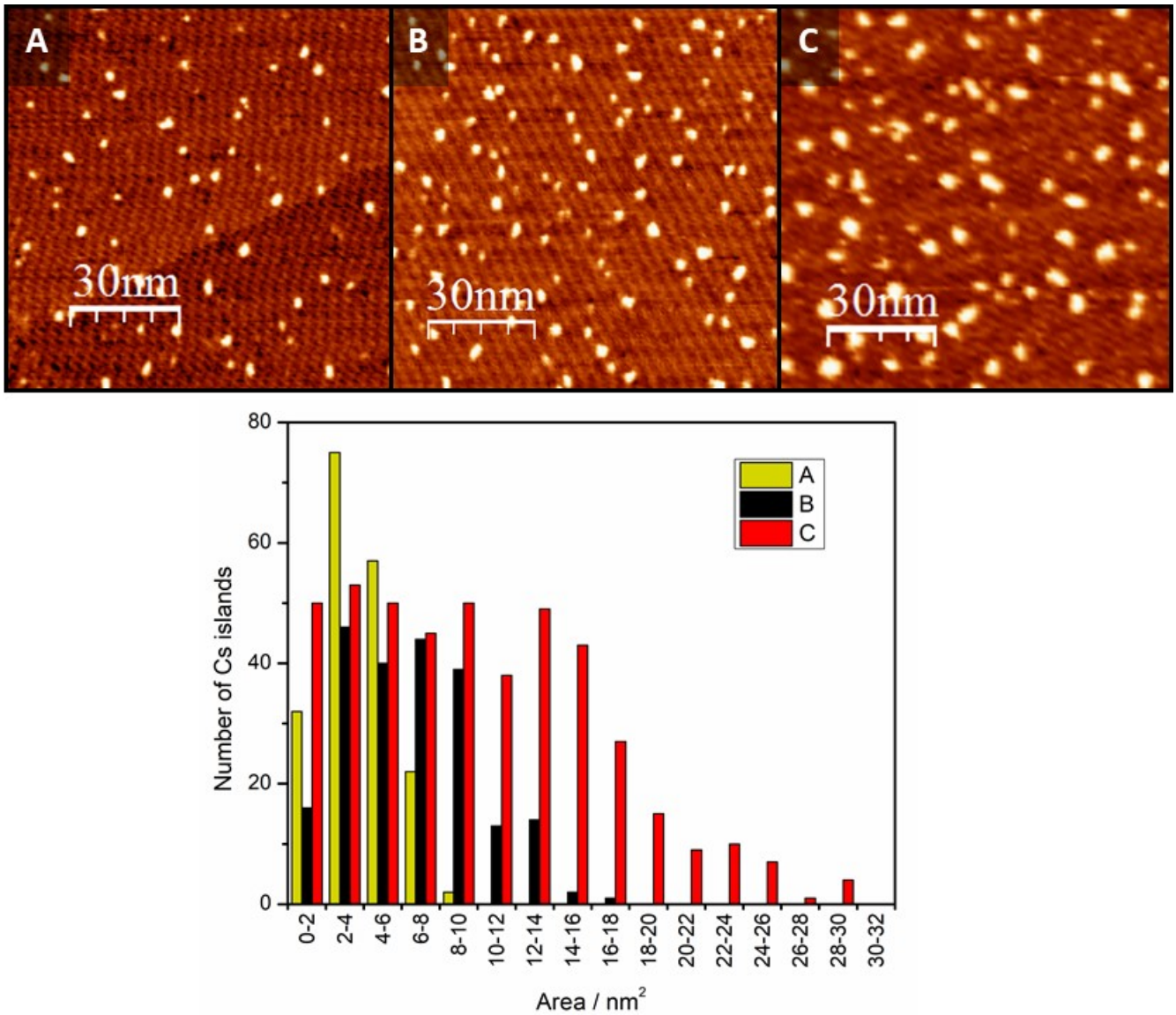

Figure S2: STM images of 3 different Cs coverages on Cu_2O/Cu(111) (Top) and below, a corresponding histogram of the Cs island area for each image. The deposition time and estimated coverages for each are as follows: A) 5 sec., 2.5%, B) 10 sec., 5.9%, and C) 15 sec., 9.2% by area.

As the amount of cesium increases, the greater the area range of the protrusions. There are small area protrusions at each coverage, but as the coverage increases, so does the size of the largest feature present. For example, at the lowest coverage of 2.5%, the largest features are 8-10 square nm. At the highest coverage of 9.2%, the area of the protrusions extends up to 28-30 square nm.

3) $Cu_2O/Cu(111)$ point defects

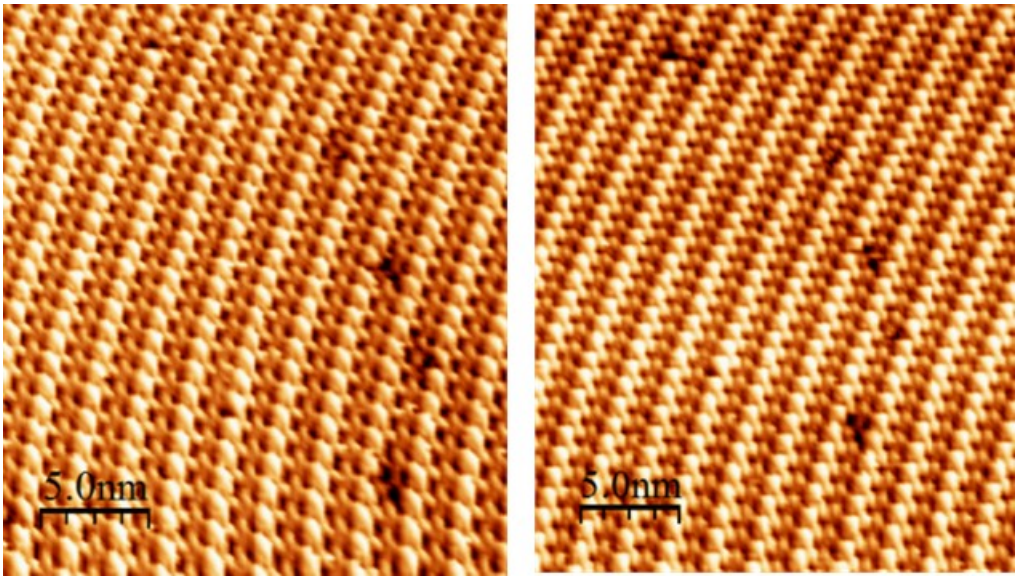

Figure S3. Sequential STM images of point defects on the $Cu_2O/Cu(111)$ surface. Without cesium, these defects do not rapidly diffuse.

4) Full Cs/Cu_xO/Cu(111) anneal

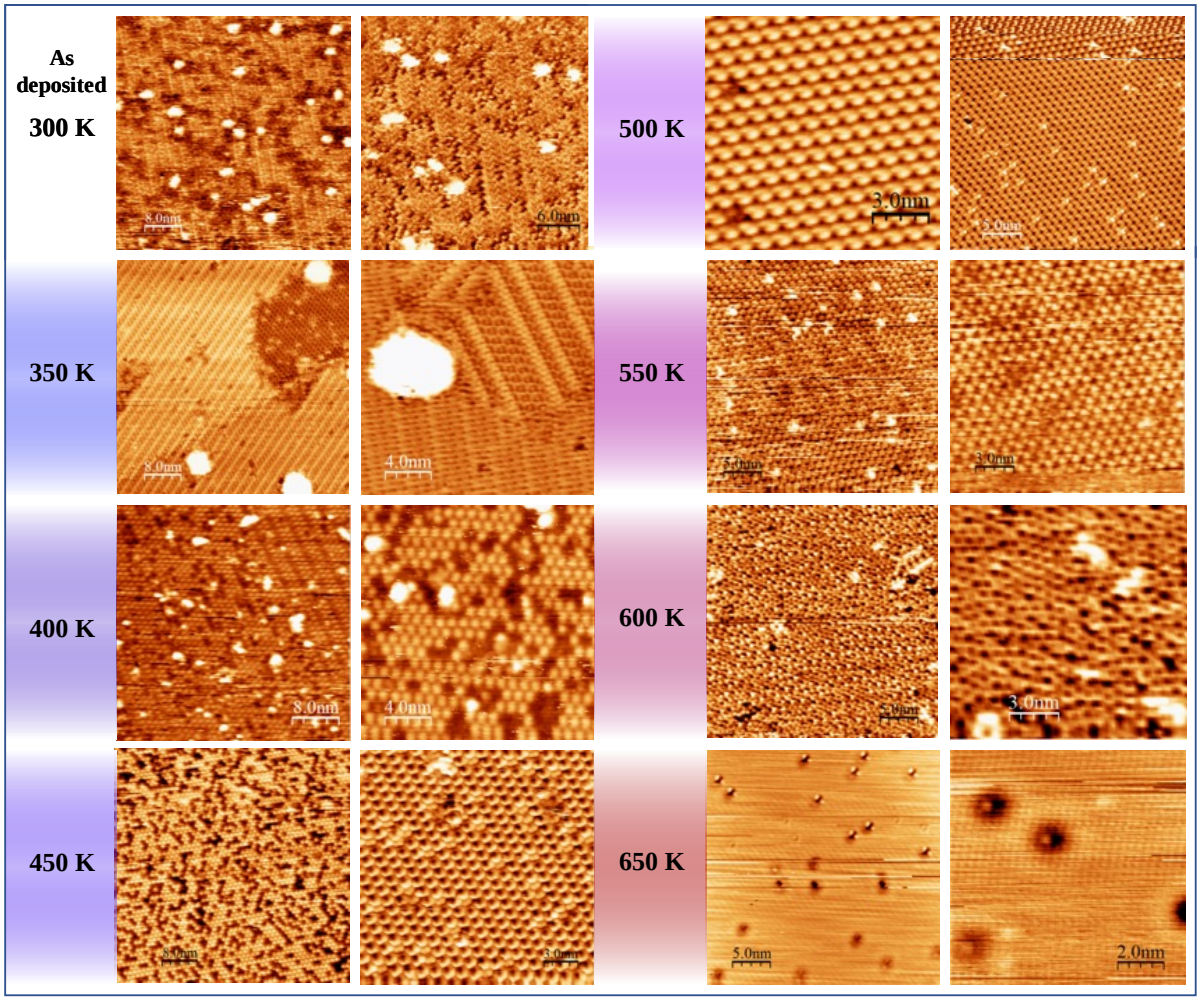

Figure S4: STM images of the full Cs/Cu_xO/Cu(111) sequential annealing process. This figure provides more information for the annealing structures, with larger and smaller scale images as well as the contrast morphologies of the hexagonal 'honeycomb' structure.

5) Lower Cs coverage anneal

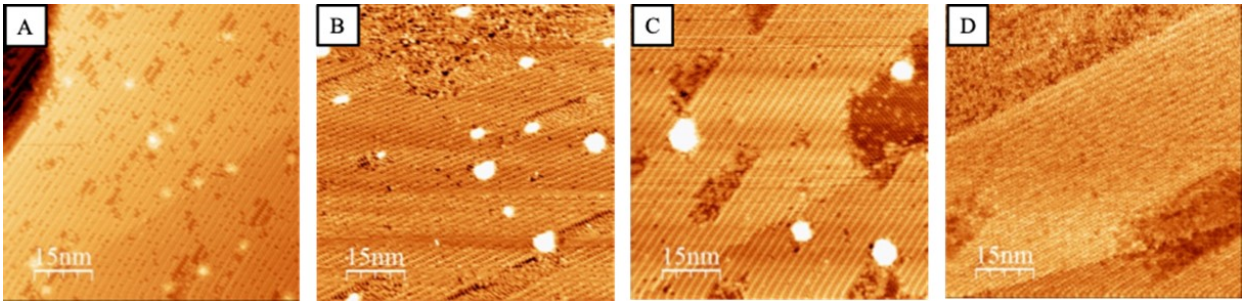

Figure S5: STM images after a gentle progressive anneal. These are taken with a lower coverage of Cs on the Cu_2O thin film so as to help ascribe the formation of the hexagonal regions with the amount of Cs on the surface. All images are 75 nm^2 and annealing conditions (5 min each) are as follows: A) I_{fil}: 1.5 A, 2.0 V, ~69 ˚C. B) I_{fil}: 2.0 A, 3.2 V, ~123 ˚C. C) I_{fil}: 2.2 A, 3.7 V, 200 ˚C. D) I_{fil}: 2.5 A, 4.2 V, 275 ˚C